THESIS FOR THE DEGREE OF DOCTOR OF PHILOSOPHY IN NATURAL SCIENCE,
SPECIALISING IN CHEMISTRY

On the Electrolyte Induced Aggregation of Concentrated Silica Dispersions

An Experimental Investigation Using the Electrospray Technique

Ann-Cathrin Johnsson

UNIVERSITY OF GOTHENBURG

Department of Chemistry
University of Gothenburg
Göteborg, Sweden, 2011

On the Electrolyte Induced Aggregation of Concentrated Silica Dispersions
An Experimental Investigation Using the Electrospray Technique

Department of Chemistry
University of Gothenburg
412 96 Göteborg, Sweden

Printed by Hylte Tryck AB
Mölndal, Sweden 2011

ISBN 978-91-628-8328-7 (available online at: http://hdl.handle.net/2077/26662)

Cover picture: Drawing of a spraying event for an aggregating system of monodisperse silica particles together with the obtained size distributions.

In loving memory of my grandfather Nils Nilsson –

A man who went to the woods and lived deep

Abstract

Gels are weak, solid-like structures that arise when colloidal particles aggregate to form a network of particle clusters. A variety of colloidal systems that are important scientifically as well as in industrial applications are capable of gel formation, *e.g.* globular protein solutions, colloid-polymer mixtures, and metal oxides. Yet, the mechanisms of the gelation process are far from understood, and the investigation of the aggregation and gelation of colloidal dispersions is, therefore, of great importance. Especially, the size distribution and structure of the aggregates are known to affect the gelation, and the main focus of this thesis is to improve our understanding of the initial aggregate formation in concentrated silica dispersions.

The electrospray-scanning mobility particle sizer (ES-SMPS) technique has previously been demonstrated to be a valuable method for size distribution analysis of pure colloidal dispersions. Here, the ES-SMPS method was used to monitor the size distribution variation during electrolyte induced slow aggregation of concentrated silica dispersions. Number size distributions provide information about the primary particles as well as the formed aggregates. The influence of the ion specificity, as well as three initial particle morphologies, on the aggregation behaviour was investigated. Moreover, the aggregate diameters obtained by the ES-SMPS method were compared to the those obtained by other techniques such as scanning electron microscopy (SEM) and *in situ* small angle X-ray scattering (SAXS).

The initial aggregate formation could be monitored accurately using the ES-SMPS method and compact, nearly spherical aggregates were observed for two of the initial morphologies. It was concluded that these resulted from a dynamic aggregation process where the aggregates broke and reformed several times prior to the gelation. More elongated aggregates were observed in the third dispersion; these aggregates were more rapidly stabilized by interparticle bonds and formed the most stable gel structures. The surface properties of the particles were found to affect the aggregate structure.

Clear ion specific effects were observed; the most stable aggregates were formed in the presence of the least hydrated alkali ions, whereas the rate of gel stability increase was faster in the presence of the more strongly hydrated ions. As expected, the alkali ions adsorbed according to the direct Hofmeister sequence.

A gel layer on the silica particle surfaces was identified for all dispersions investigated. The thickness of these layers were estimated using different techniques and found to be 2-4 nm thick depending on the dispersion.

Keywords: Colloidal silica dispersion, aggregation, gelation, electrospray (ES), scanning mobility particle sizer (SMPS), synchrotron radiation small-angle x-ray scattering (SR-SAXS), electron microscopy (EM), dynamic light scattering (DLS), particle morphology, ion specificity, gel layer

List of Publications

This thesis is based on the work presented in the following papers. In the text the papers will be referred to by their Roman numerals.

Paper I

Aggregation of Nanosized Colloidal Silica in the Presence of Various Alkali Cations Investigated by the Electrospray Technique

A.-C. J. H Johnson, P. Greenwood, M. Hagström, Z. Abbas, and S. Wall
Langmuir, **2008**, 24, 12798-12806.

Paper II

Combined Electrospray-SMPS and SR-SAXS Investigation of Colloidal Silica Aggregation. Part I. Influence of Starting Material on Gel Morphology

A.-C. J. H. Johnsson, M. C. Camerani, and Z. Abbas
J. Phys. Chem. B, **2011**, 115, 765-775.

Paper III

Combined Electrospray-SMPS and SR-SAXS Investigation of Colloidal Silica Aggregation. Part II. Influence of Aggregation Initiator on Gel Stability

A.-C. J. H. Johnsson, M. C. Camerani, and Z. Abbas
J. Phys. Chem. B, **2011**, 115, 9547-9555

Paper IV

Intermethod Comparative Analysis of the Particle Size Distributions of Colloidal Silica Nanoparticles

J. Tuoriniemi, A.-C. J. H. Johnsson, J. Perez Holmberg, S. Gustafsson, J. Gallego, E. Olsson, J. B. C. Pettersson, and M. Hassellöv
Manuscript for *Langmuir*

Statement of Contribution

Paper I

Formulated the research problem with support from co-authors, designed and performed all experiments, preformed the SEM imaging, responsible for all data evaluation, lead author with support from co-authors.

Paper II

Major contribution to the formulation of the research problem, designed and preformed all ES-SMPS experiments, preformed the SEM imaging, major contribution to the data evaluation, lead author with support from co-authors.

Paper III

Major contribution to the formulation of the research problem, designed and preformed all ES-SMPS experiments, major contribution to the data evaluation, lead author with support from co-authors.

Paper IV

Performed ES-SMPS experiments and the SEM imaging, major contribution to the evaluation and interpretation of the data, contributed to the writing of the manuscript.

Table of Contents

List of Abbreviations

CCC	Critical Coagulation Concentration
CPC	Condensation Particle Counter
DLS	Dynamic Light Scattering
DLVO	Derjaguin, Landau, Verwey and Overbeek
d_m	Mobility diameter
DMA	Differential Mobility Analyzer
d_p	Physical diameter
d_{ve}	Volume equivalent diameter
EM	Electron Microscopy
ES	Electrospray
FFF	Flow Field Fractionation
FTP	Fraction of Total number of Particles
HS	Hard Sphere
IEP	Isoelectric Point
IIC	Ion-Ion Correlation
MC	Monte Carlo
NTA	Nano Tracking Analysis
PoG	Point of Gelation
PSD	Particle Size Distribution
SAXS	Small-Angle X-ray Scattering
SE	Secondary Electrons
SEM	Scanning Electron Microscopy
SMPS	Scanning Mobility Particle Sizer
SR	Synchrotron Radiation
TEM	Transmission Electron Microscopy

Chapter 1

Introduction

1.1 Colloidal Dispersions

Colloidal dispersions are important in everyday life, and can frequently be found in a number of diverse products, such as milk and eggs,[1] or hygiene products;[2] in paint and ink;[3] and even in our own bodies as some properties of blood are best described by considering it as a colloidal dispersion.[4] But what is a colloidal dispersion?

A system which contains particles that are immiscible with, and suspended in, a continuous medium, *e.g.* water droplets suspended in air which form a cloud, is by definition a dispersion. These systems are usually regarded as colloidal if the particle size is in the 1-1000 nm range, however, there exists dispersed systems where the particles are larger.[4,5] The particles, also called the disperse phase, may be a solid, a liquid, or a gas, as can the dispersion medium and a number of possible combinations arise. In fact, the only combination not found is the gas-gas dispersion, which is impossible because all gases are mutually miscible. This thesis concerns two specific dispersions – aerosols: solid or liquid particles dispersed in a gas, and hydrosols: solid particles dispersed in a liquid – and, in particular, the possibilities to investigate important properties of the latter by transferring it into the former.

The small dimensions of the dispersed phase lead to a large contact area between the particles and the continuous phase – a distinguishing feature of all colloidal systems. A significant amount of energy is associated with the creation and preservation of an interface. Many colloidal dispersions are, therefore, unstable in the sense that the system constantly strives to reduce the contact area – the particles form aggregates. Gelation occurs if the particles aggregate to form a network of particle clusters, this process results in the formation of solid-like structures called gels.[6] Many industrial processes involving colloidal dispersions, often with high particle concentrations, require highly stable dispersions. To maintain the stability of the dispersed phase the particle surfaces may be modified to provide electrostatic and/or steric energy barriers that prevent aggregation.

Aqueous colloidal silica dispersions, silica sols, play an important role in a number of industrial applications, such as silicon wafer polishing, coating applications, and chemical mechanical planarization;[7,8] which all require well defined, stable dispersions. In some applications, it is the aggregation itself, or rather the structures resulting from this process (*e.g.* flocs or gels), that is the desired result. These include, for instance, flocculation applications such as beverage fining and paper-making;[7,9] furthermore, the gelling dispersions can be used as a grouting material[10,11] or as a soil stabilizer,[12] and the

resulting gel structures as solid state electrochemical devices.[13] In either case, whether the aggregation is desired or not, the aggregation behaviour as well as the particle size and size distribution are of utmost importance to the performance of the silica sols. In addition, silica is often used as a model system in contact angle and surface force measurements, or to study aggregation and rheology; and the material has been extensively investigated for decades.[7,9] Nevertheless, the aggregation and gelation mechanisms as well as the properties of the silica-water interface are not fully unravelled.[14-19]

Central parameters that will affect the aggregation are, among other things, the shape, size and interaction of the particles in the dispersion. The size and shape of the particles can influence the aggregate and gel structures directly, as the actual physical dimensions of the particles (to some extent) determine their possible positions in the structures, and indirectly because these parameters also affect the particle interactions. The aggregate shapes appear particularly relevant to the alternative development of an arrested state (a gel) or gas-liquid phase transition.[20] Additional interparticle attraction, apart from the van der Waals interaction, can be introduced by the addition of an electrolyte or polymers. This will also affect the structure and microscopic properties of the aggregates, particularly in the early stages of the aggregation.[21,22]

Generally, particles in a real system have a distribution of sizes, wherefore particle size distribution (PSD) measurements are an integral part of colloidal studies. Naturally, many methods have been developed,[4] but only a few of these offer the possibility to obtain number size distributions. In addition, some of the methods that do, *e.g.* electron microscopy, require time-consuming procedures to obtain reliable distributions. In recent years, a new technique that utilizes well-defined aerosol methods to obtain number size distributions of hydrosol particles have been developed.[23-25] The particles are transferred to the gas phase by means of electrospray (ES); subsequently, the particles are classified according to their mobility in air, and counted, using a scanning mobility particle sizer (SMPS). Lenggoro et al. showed that accurate size distributions could be obtained for a number of pure colloidal dispersions using the ES-SMPS method.[26] One important aspect of this method is that no assumptions concerning the shape of the size distributions are made *a priori*. Moreover, this technique may offer the possibility to separate the signal originating from the aggregates from that of the primary particles. These appealing features makes the ES-SMPS method a good candidate for aggregation analysis, and especially for studying the very onset of aggregation.

1.2 Purpose of the Thesis

The overall aim of the work presented in this thesis was to improve our understanding of the mechanisms involved in the initial aggregate formation during electrolyte induced aggregation of concentrated colloidal silica dispersions. An additional aim was to investigate the effects of ion specificity and initial particle morphology on the structure and strength increase of the obtained gel networks.

A procedure for electrospray-scanning mobility particle sizer (ES-SMPS) analysis on aggregating dispersions was developed and applied to the aggregation of spherical silica particles in the presence of various alkali ions (Paper I). This is an invasive method because the concentrated dispersions have to be diluted prior to analysis. Thus, to verify the results obtained using the ES-SMPS method, the aggregation was also monitored with small-angle X-ray scattering which is a non-invasive method (Papers II and III). In addition, the effects of initial particle morphology as well as the choice of anion were examined in these papers.

The aggregation behaviour of silica dispersions is strongly affected by the surface properties of the particles and the structure of the silica/aqueous electrolyte interface. Thus, to gain a better insight to the structure of silica particle surface, the size distribution of a pure silica dispersion was measured using multiple techniques, including scanning electron microscopy (SEM), transmission electron microscopy (TEM), and dynamic light scattering (DLS). The results of the different measurements were analysed collectively to offer a coherent depiction of the particle properties (Paper IV).

1.3 Outline of the Thesis

The work that serves as a basis for this thesis has resulted in four scientific papers. To put the results in context, a background to the field of interest is presented in Chapter 2. This includes an overview of the standard theory of colloidal stability and additional interactions that may affect the overall stability. A description of the silica system and the particle surface properties, along with a summary of silica aggregation, is given. The central parameters of size distributions, and some important theoretical distributions, are also discussed.

This thesis concerns the development, validation, and application of a new procedure for the analysis of colloidal silica aggregation by means of the ES-SMPS technique. In Chapter 3 a description of the ES-SMPS system is given, and analysis of colloidal systems using this technique is described. Several techniques traditionally used in colloidal analysis were used to verify the results obtained from the ES-SMPS analysis. Therefore, short descriptions of these techniques: Small-Angle X-ray Scattering (SAXS), Scanning and Transmission Electron Microscopy (SEM and TEM), as well as Dynamic Light Scattering (DLS), are given.

The results from the four papers are summarized in Chapter 4; beginning with a summary of the particle characterization results obtained for the dispersions included in Papers I-IV (section 4.1). This includes a more detailed analysis of the PSD of one of the pure dispersions with respect to the effect of the silica particle surface properties on the

particle sizes obtained with various methods. The dissolution of the silica particles stored in highly diluted solutions will be discussed in section 4.1.2. The procedure for aggregation analysis with the ES-SMPS setup, developed in Paper I, is presented in section 4.2. The aggregation was observed to be fully reversible and the aggregate disintegration results are also presented in 4.2, along with a comparison of the aggregate diameters obtained using the ES-SMPS method, SEM, and *in situ* SAXS measurements. The effects of initial particle morphology on the aggregate formation was investigated in Paper II, and the sequential build-up of the initial aggregate structures for three initial particle morphologies are discussed in section 4.3. In section 4.3.3, a suggestion concerning gel network structures that could result from these aggregate structures is presented, and compared to existing suggestions for silica gel networks. The ion adsorption sequence was determined and the ion specific effects observed in Papers I-III are discussed in section 4.4. Finally, a summary of the conclusions presented in the thesis, along with some suggestions for future studies, are given in Chapter 5

Chapter 2

Background

2.1 Theory of Colloidal Stability

A colloidal dispersion is considered stable if the particles in the dispersion remain separated for long periods of time, on the order of days as a lower limit. The dispersion can be stabilised thermodynamically or kinetically.[27] In the former case the dispersion has a lower Gibbs free energy as compared to its separated constituents. For instance, dried-out lyophilic (solvent loving) colloids, such as proteins or polysaccharides, will spontaneously re-disperse if subjected to the solvent; these systems are thermodynamically stable. However, most dispersions contain lyophobic (solvent hating) particles and these systems are kinetically stabilised. The particles are attracted to one another by van der Waals interactions and, although aggregation is delayed by an energy barrier, given sufficient time the system will inevitably coagulate. The stability of lyophobic colloids can be described by the classic DLVO-theory,[4,28,29] named after the scientists Derjaguin, Landau, Verwey, and Overbeek who developed this theory.[30,31]

2.1.1 The DLVO Theory

In the vicinity of a charged surface oppositely charged ions are enriched in a diffuse layer; together the surface and the diffuse layer constitute an electro-neutral entity. When two charged surfaces approach each other their diffuse layers start to overlap. The overlap gives rise to an osmotic pressure between the surfaces; a repulsive electrostatic interaction separates the surfaces by opposing further approach. For two weakly interacting spherical particles of equal size, the interaction energy, V_R, is given by:[32]

$$V_R(h) = \frac{32\pi\varepsilon_r\varepsilon_0 r (k_B T)^2 \gamma_0^2}{e_0^2} \cdot e^{(-\kappa h)}; \quad \text{(for 1:1 electrolytes)} \tag{1}$$

where ε_0 is the vacuum permittivity, ε_r is the dielectric constant of the medium, r is the particle radius, and h is the particle centre-to-centre distance. k_B and T are the Boltzmann constant and the temperature, respectively; e_0 is the electronic charge, and κ and γ_0 are given by:[32,33]

$$\kappa = \left(\frac{e^2 \sum_i n_i^0 z_i^2}{\varepsilon_r \varepsilon_0 k_B T} \right)^{1/2} \quad \text{and} \tag{2a}$$

$$\gamma_0 = \tanh\left(\frac{z e_0 \psi_0}{4 k_B T} \right) \tag{2b}$$

where ψ_0 is the surface potential, and n_i^0 and z_i are the bulk concentration and valency of species i, respectively. It can be seen that, apart from fundamental constants, the Debye-Hückel parameter, κ, depends solely on the bulk electrolyte concentration and the temperature. The inverse of this parameter, κ^{-1}, known as the Debye length, is a measure of the thickness of the diffuse layer.

The attractive van der Waals interactions, which constantly strive to coagulate the particles in dispersions, originate from the polarisability of the atoms that constitute the particles. A significant contribution to the attractive interactions is made by the dispersion interaction, which can be understood to result from the virtual fluctuations in the instantaneous positions of the electrons surrounding the atoms. Consider two interacting particles in a dispersion; every atom in particle one exerts a force on the atoms in particle two and vice versa. Hamaker obtained an expression of the overall interparticle attraction by summing up these pair-wise contributions.[34] The van der Waals interaction energy, V_A, between two spherical particles of radius, r, is given by:[35]

$$V_A(h) = \frac{A \cdot r}{12h} \tag{3}$$

where A is the Hamaker constant. In the DLVO-theory the total energy of the interaction between the particles is estimated as the sum of the repulsive contribution due to the electrostatic interaction and the van der Waals attraction:

$$V_{tot} = V_R + V_A \tag{4}$$

The main features of the theory can be summarised as follows:[29]

- Particles of materials with large Hamaker constants will display a strong attraction.
- A high surface potential renders a greater repulsion between the particles and thus a more stable dispersion. Consequently, the dispersion is predicted to be completely destabilized at the isoelectric point (IEP).
- An increase of the bulk electrolyte concentration will compress the diffuse layer and the apparent surface potential decreases, this leads to a decrease in the electrostatic repulsion.

The decrease of the electrostatic repulsion will diminish the electrostatic energy barrier that prevents aggregation. This is depicted schematically in Figure 1, where a) illustrates the system prior to electrolyte addition; b) corresponds to the electrolyte concentration a which the energy barrier has just disappeared, also known as the critical coagulation concentration (CCC); c) the bulk electrolyte concentration is sufficiently high to completely reduce the energy barrier. The CCC is an important parameter in aggregation studies, as it constitutes the dividing line between slow and fast aggregation. This will be further discussed in section 2.4.2.

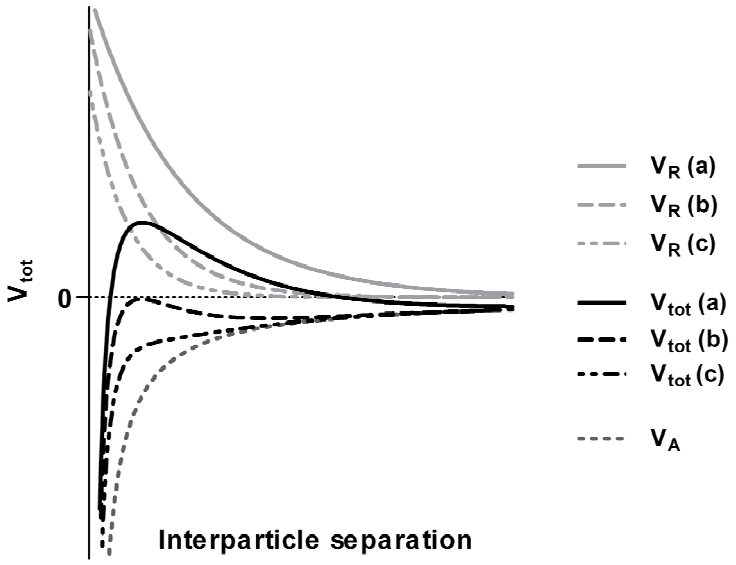

Figure 1. A schematic of the decrease in the total energy of interaction between two particles, V_{tot}, upon electrolyte addition. a) no electrolyte added, b) the critical coagulation concentration, and c) sufficient amount of electrolyte added to completely reduce the energy barrier. The total energy of interaction was calculated according to the DLVO-theory.

2.2 Non-DLVO Interactions

Although the DLVO-theory has been shown to work well for number of colloidal systems,[36-40] the theory fails to explain the behaviour of some specific systems owing to the fact that the theory neglects a number of interactions.[41-43] First of all, the solvent is regarded as a dielectric continuum, and any solvent–solvent and surface–solvent interactions are neglected. This means that additional repulsion, V_{Solv}, which can be observed for surfaces with a highly structured hydration layer, is disregarded; as is the steric repulsion, V_{Ster}, which occurs, for instance, when surfaces with grafted polymers approach each other. Furthermore, ionic species are regarded as point charges, which results in an inaccurate estimation of the ion–surface, ion–ion, and ion–solvent interactions. Thus, according to the classical theory, ions can approach the surface infinitely, and equal concentrations of equicharged ions should affect the system identically. Nevertheless, it is frequently observed that not only the charge but also the choice of electrolyte affects, for instance, how efficiently the charge of a surface is screened. This effect is known as ion specificity and its main features will be summarized in the following section.

2.2.1 Ion Specificity

Ion specific effects were first discovered by Hofmeister,[44] who arranged anions in a sequence according to their efficiency in salting out egg white. Since then they have been observed in various experiments, such as bubble fusion,[45] bacterial cell growth,[46] surface tensions of electrolytes,[47,48] charge of globular proteins,[49] as well as yield stress and IEP-shift in silica suspensions.[17] With respect to colloidal stability, ion specific adsorption is especially important because ions that adsorb close to the surface will have a high screening efficiency; consequently, a lower electrolyte concentration is required to destabilize the dispersion.[50] In all experiments presented here the counterions were alkali ions. If the surface affinity of these ions increases according to $Li^+ < Na^+ < K^+ < Rb^+$

< Cs^+, the direct (Hofmeister) sequence is observed.[51] The reversed order, Li^+ is preferentially adsorbed as compared to Cs^+, is referred to as the indirect sequence. A classical explanation of the ion absorbability is given by the Stern model: The adsorption of an ion is determined by its electrical charge and its size; highly charged ions adsorb more strongly and, in the case of equicharged ions, small ions are preferentially adsorbed compared to large. However, this model is unable to explain, for instance, the observed reversal of the adsorption sequence of alkali ions at a mercury/water interface with preadsorbed pyridine.[52,53]

Ninham et al.,[54] and others,[55-58] have shown that most ion specific effects can be explained theoretically by including the ion-ion and ion-surface dispersion interactions. Nevertheless, these interactions are unable to explain the results obtained by Dumont et al.[59] In a classic paper they showed that the adsorption sequence at the TiO_2/water interface could be reversed by varying the IEP of the TiO_2 sample. This indicates that ion specific effects are not solely due to additional dispersion interactions, because the Hamaker constants of the samples are identical. Rather, it is the change of the surface water structure, associated with the IEP shift, that gives rise to the inversed adsorption.[51]

Based on their interaction with the solvent, ions can be classified in two main groups.[60,61] Ions that promote water structure in their vicinity, such as Li^+ and Na^+, are known as structure-maker ions. For structure-breaker ions the solvent becomes less structured in the vicinity of the ion, as compared to the bulk phase. Similarly, particle surfaces can be classified according to their ability to promote or destroy the surrounding water structure, referred to as structure-maker or structure-breaker surfaces, respectively.[59,62] The adsorption sequences observed for a number of oxides can be explained by a "like seeks like" concept. Oxides with a high IEP, *e.g.* alumina or rutile, are structure-maker surfaces and structure-maker ions preferentially adsorb on these surfaces, whereas structure-breaker ions preferentially adsorb on low-IEP oxides such as silica.[17,59] Recently, Parsons and co-workers showed that inversion of the adsorption sequence can be explained theoretically, provided that both the ion-surface dispersion interactions and ion hydration are included.[63] If these interactions oppose one another, however, the adsorption will be governed by the compatibility of the ion and surface water structures, as demonstrated by Lopéz-Léon et al.[64] For planar silica substrates the ion specific effects of monovalent alkali ions are weak,[65] whereas the effect can be quite substantial for colloidal silica.[17]

It can be shown that ion-ion interactions in the double layer lead to an attractive electrostatic pressure contribution to the double layer interaction between two surfaces.[66,67] Provided that this constitutes the dominant contribution a short-range attractive ion-ion correlation (IIC) interaction will be observed. The attraction arises due to charge fluctuations in the system, thus, its mechanism is similar to that of the dispersion interaction, but it is often much stronger than the van der Waals attraction. The magnitude of the electrostatic pressure contribution is almost independent of the valency of the counterions.[66,68] For high ion densities between two approaching surfaces the double layer interaction is repulsive at all distances. However, if the ions can approach the surface sufficiently close, so that the ion density at the midplane is

substantially reduced, the attractive part will dominate. Thus, the additional short range electrostatic IIC attraction interaction may be observed in systems with strongly adsorbed ions.

2.3 Particle Size Distribution

One of the most important features of a dispersion is the shape and size distribution of the particles in the system as these, to some extent, affect almost all other properties of that system. If the dispersion contains particles of one size only, it is said to be monodisperse. In theoretical calculations, particles are usually assumed to be monodisperse and spherical for simplicity. Real systems contain particles that vary in size, *i.e.* the system shows a degree of polydispersity.

A perfectly monodisperse dispersion can be described by the δ-function, while for all other systems a size distribution has to be constructed; the size range of interest is divided into intervals and the particles in each interval are counted. A distribution can be weighted by different parameters, such as number or mass. The first moment of a distribution is the mean and the second moment is the variance, σ^2; the polydispersity, p, of the distribution is defined as the square root of the ratio of the second moment and the square of the first moment. For example, the number mean diameter, $\bar{d}$, is defined as:[69]

$$\bar{d} = \frac{\sum n_i d_i}{\sum n_i} \tag{5}$$

where n_i is the number of particles in size interval i, and the variance is given by: [69]

$$\sigma^2 = \frac{\sum n_i \left(d_i - \bar{d}\right)^2}{\sum n_i} \tag{6}$$

Thus, the polydispersity of this distribution is equal to $\sigma/\bar{d}$. The most important characteristics of a dispersion are the mean and standard deviation, σ, which is the square root of the variance.

Theoretical distributions, such as the Gaussian or log Gaussian, can be used to describe the PSD. In Papers II and III, the Schulz distribution was used in the interpretation of the SAXS data. This distribution is defined as:[70]

$$S(r) = \frac{r^z}{\Gamma(z+1)}\left(\frac{z+1}{\bar{r}}\right)^{z+1} e^{\left(-\left[\frac{r(z+1)}{\bar{r}}\right]\right)}, \quad z > -1 \tag{7}$$

where r is the particle radius, $\Gamma(x)$ is the Gamma function, and z is a width parameter. The shape of this distribution varies with the value of z; for small z-values it resembles a log Gaussian, when z increases the distribution becomes progressively more narrow and Gaussian 'like', and as z approaches infinity it becomes a delta function at $r = \bar{r}$.[70]

When a dispersion starts to aggregate, it will contain the newly formed aggregates as well as unaggregated initial particles. In that case, the real PSD of the system will contain (at least) two modal sizes. Provided that the analysis method used can separate these fractions, a bimodal or polymodal PSD may be obtained. The PSD can then be estimated as the sum of two or more theoretical distributions.[71]

2.4 Colloidal Silica Dispersions

"Silicon dioxide is the main component of the crust of the earth. Combined with the oxides of magnesium, aluminium, calcium, and iron, it forms the silicate minerals in our rocks and soil." – Ralph K. Iler

A colloidal silica dispersion consists of amorphous silicon dioxide particles dispersed in water. The structure of silicon dioxide, or silica for short, is based on a network of SiO_4 tetrahedra with shared oxygen atoms. The arrangement of the tetrahedral units determines the structure of the silica material. Various crystalline silicas, such as quartz, cristobalite, and tridymite, can be formed from the ordered arrangement of SiO_4; whilst a random packing of the tetrahedrons results in amorphous silica.[7,9]

Silica particles can, for instance, be formed via the hydrolysis and subsequent condensation of alcoxysilanes. This synthesis was first described by Stöber et al.[72] and the resulting dispersions of porous silica particles are often referred to as Stöber sols. An alternative silica precursor source is dilute aqueous water-glass solutions. The dispersions that are investigated in this thesis were synthesized via the ion exchange method. In this method an active silicic acid solution is formed by allowing the water-glass solution to pass through an ion exchange column. Subsequently, nucleation, polymerisation, and particle growth is initiated by the addition of alkali at temperatures above 60 °C. By varying different parameters, such as temperature, pH, and the molar ratio of SiO_2:Na_2O, dispersions with various particle morphologies can be obtained.

Silica dispersions are used in a vast number of applications, which can be subdivided into binding and non-binding applications.[9] Silicon wafer polishing is an example of a non-binding application. In this case a well defined particle size distribution is vital for the overall performance. In binding applications, such as paper making, flocculation, and catalyst manufacturing, a well-known and controlled aggregation behaviour of the particles is essential.[7,9] In recent years a new area of use, where the particle aggregation is of importance, has emerged; a silica dispersion is destabilised and the gelling system is used as a grouting material in hard rocks or soils.[10-12]

2.4.1 Surface Properties

On the surface of the silica particles, silanol groups, Si-OH, are formed, and in aqueous silica dispersions the particle surface charge is established by protonation and deprotonation of these groups according to the following reactions:[73]

$$\begin{aligned} Si-OH + H^+ &\leftrightarrow Si-OH_2^+ \\ Si-OH + OH^- &\leftrightarrow Si-O^- + H_2O \end{aligned} \qquad [1]$$

Compared to other oxides, these particles have a low isoelectric point (IEP), and they are negatively charged above pH 2. The surface charge density rises steeply with increasing pH and, depending on the counter ion present, these surfaces can attain very high charge densities.[74] Meanwhile, the zeta potential can be quite low owing to the fact that adsorbed counterions compensate (to some extent) the surface charge.[74,75]

At a low pH, the silica surface is well hydrated because water molecules can be hydrogen bonded to the silanol groups.[76] Generally, the silica surface is regarded as a structure-

breaker surface with the ability to disrupt the adjacent water structure (*cf.* the discussion concerning structure-maker and structure-breaker ions in section 2.2.1). At first, this may seem counter intuitive; a well-hydrated surface with the ability to disrupt water structure. However, if we compare silica to *e.g.* mica, which has a hydration layer with an almost 'ice-like' structure,[77] the silica surface has a rougher structure owing to the fact that this material is amorphous. The hydrogen-bonded water molecules at the silica surface will be oriented in a broader distribution of directions, giving rise to a disrupted water structure.[78] With increasing pH the surface hydration will decrease due to the deprotonation.

It has been proposed that a so-called gel layer, consisting of protruding and/or adsorbed polysilicic acid chains, forms at the surface of the particles.[14,79,80] The results obtained by Vigil et al. suggest that the gel layer is approximately 1 nm thick.[14] Furthermore, smaller particles are thought to have a thicker gel layer as compared to larger particles.[80] The presence of such a layer would further increase the roughness of the surface, thereby increasing its structure-breaker character. In addition, the layer will act as a steric barrier, thus enhancing the stability of the dispersion.

According to the DLVO-theory, dispersions are unstable at the IEP, because the electrostatic repulsion that stabilizes the dispersion disappears. However, colloidal silica dispersions display an unusual stability behaviour with a stability maximum at the IEP and a stability minimum in the intermediate pH range (pH 4-7). In some cases, additional repulsive non-DLVO interactions have also been observed in the high pH range.[80] Over the years, both the hydration of the surface and the gel layer have been put forward as explanations for the remarkable stability of the silica system. Most likely, the behaviour can be attributed to a combination of the two mechanisms. In the low pH range (< 4), where the surface is strongly hydrated, the repulsion due to hydration layer overlap is more important. With increasing pH, the surface is dehydrated and the surface charge starts to increase;[81-83] this will inflate the gel layer because the charges within the layer are repelled by one another and by the charges on the surface.[14] A low stability in the intermediate region is observed because the decrease of the hydration layer repulsion is faster than the increase of the electrosteric repulsion.[83] Most likely, the gel layer overlap represents a major contribution any additional repulsion observed at high pH (> 8), because the silica surface has a low degree of hydration above pH 7. [81-83]

2.4.2 Silica Aggregation

Silica dispersions prepared by the ion exchange method are very stable owing to the low concentration of destabilising contaminants; the shelf time for a concentrated system (pH 8-10) is on the order of 6-12 months, depending on the specific surface area of the dispersion. However, when required, *e.g* in applications such as rock grouting, aggregation can be induced in a number of ways, of which the most simple is to decrease the pH. Furthermore, the addition of polymers may induce flocculation,[84] and electrolyte addition will increase the bulk electrolyte concentration, whereby the electrostatic repulsion is screened due to the compression of the diffuse layer. [29]

Aggregation as such can be subdivided into a slow and a fast regime; the critical coagulation concentration, CCC, represent the division between the two. The CCC is the

bulk electrolyte concentration at which the electrostatic repulsion has been screened to the point where the energy barrier, which prevents aggregation, has only just disappeared. Devoid of an energy barrier, the rate limiting step is the transportation of primary particles to the growing clusters; in an unstirred system, the particles are transported by diffusion and fast aggregation occurs. Below the CCC, the rate limiting step is the particle inter-collisions and the aggregation is slow.

As the aggregation proceeds, the aggregates will grow by addition of primary particles, in addition, agglomerates are formed when the aggregates adhere to other aggregates. This process continues until a network that spans the entire volume is formed. The resulting solid-like structure is usually referred to as a gel. Fast aggregation leads to elongated, fractal aggregates;[85] which results in a strong gel structure because the gel network is highly cross-linked. In the slow regime, a number of particle collisions are required to form the aggregates, which are spherical and more compact, and the resulting gel structure is weak. The work presented in this thesis concerns the slow aggregation of concentrated silica dispersions induced by electrolyte addition.

Following the DLVO-theory, aggregates should be stabilised in the primary minima by van der Waals interactions. However, silica has a low Hamaker constant, which results in a weak attraction energy. In addition, the constant can be decreased further by electrolyte addition. Primarily, the reason for this is the screening of the static part of the Hamaker constant, but the dispersive part is affected as well since the refractive index of the solution increases.[86,87] An alternative mechanism for the stabilization of silica aggregates was suggested by Depasse and Watillon; upon particle contact the silanol surface groups form inter-particle covalent siloxane bonds according to the following reaction:[88]

$$\equiv Si–OH + {}^{-}O–Si\equiv \leftrightarrow \equiv Si–O–Si\equiv + OH^{-} \qquad [2]$$

The formation of covalent bonds should lead to stable aggregates and irreversible aggregation. However, the silica surface is highly dynamical and structural reformation of siloxane bonds can readily occur because only a small amount of energy is required to break the bonds.[15,89] In fact, it was observed that the aggregation was initially reversible.[88] Given time, the number of inter-particle bonds will increase and the aggregates will become more stable.

Chapter 3

Experimental Techniques

In this chapter the ES-SMPS technique, the central experimental setup used in the investigations, will be described in detail. In addition, Small-Angle X-ray Scattering (SAXS), used in Papers II and III, and Electron Microscopy, used in Papers I-IV, will be described as these were the methods most extensively used for result validation. An interesting feature of the silica particles can be captured when results from Dynamic Light Scattering (DLS) measurements are compared with, for instance, ES-SMPS results. Therefore, a short summary of the DLS technique will also be given. Two additional methods were used in one of the investigations, Flow Field Fractionation (FFF) and Nano Tracking Analysis (NTA); these methods are described in Paper IV. The Monte Carlo (MC) simulations performed in Paper III are described in the paper.

3.1 Electrospray – Scanning Mobility Particle Sizer

The phenomenon that occurs when high voltages are applied to the meniscus of a conducting liquid was first described by Zeleny in the beginning of the 20th century.[90] This phenomenon is known as electrohydrodynamic spraying, but more commonly referred to as electrospray (ES).[91] In a classic paper, Fenn et al. showed that ES can be used to produce gas phase ions of biological macromolecules from solution.[92] Nowadays, ES is commonly used as ionisation source in mass spectrometry.[93] The technique is regarded as a gentle ionisation method, for instance, it has been shown that proteins with weakly associated subunits can be transferred intact.[94,95] Since colloidal particles can be transferred from the liquid phase to the gas phase, whereby a polydisperse aerosol is created, it is possible to determine the PSD using standard aerosol measurement techniques.[23,25,26] The dry polydisperse aerosol, consisting of colloidal particles and evaporation residues, generated by the ES unit is analysed using a SMPS system. The two major components of this system are the Differential Mobility Analyzer (DMA), where the particles are separated according to their electric mobility in air, and a Condensation Particle Counter (CPC), where the selected particles are counted.

3.1.1 Electrospray

In the ES unit, the liquid is supported at the tip of a capillary which acts as an electrode. A plate counter electrode is situated at a small distance from the tip. This point-plate electrode geometry, where the electric field is concentrated at the capillary tip, makes it easier to achieve the field strengths required to spray high surface tension liquids (such as water). A schematic of the ES setup is shown in Figure 2. When the voltage is applied, the liquid will be extracted towards the opposing electrode. In a specific voltage range,

the liquid forms a so-called Taylor cone.[96] From the apex of the cone a jet of droplets is emitted; the electrospray is operating in the cone-jet mode.

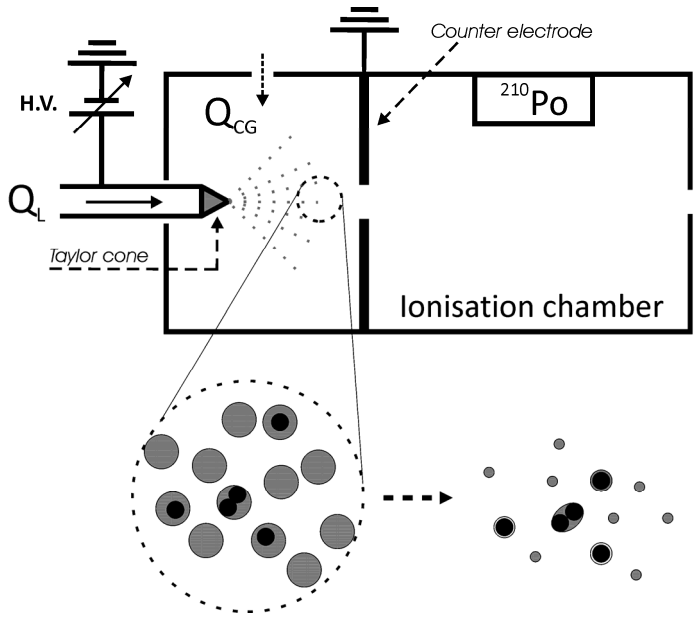

Figure 2. A schematic of the electrospray setup with the ionisation chamber. Q_{CG} is the carrier gas flow and Q_L is the liquid flow rate. The droplet evaporation process is depicted below the setup; the large gray circles are the initial droplets that evaporate to form evaporation residues (small gray circles). The black circles are the colloidal particles, when two or more particles are trapped in one droplet an aggregate is formed.

The formed aerosol is mixed with a carrier gas consisting of a particle free air/CO_2 mixture (Q_{CG}), and the solvent starts to evaporate. Initially, the emitted droplets are highly charged due to the high field strength applied at the capillary tip. As the solvent evaporates, the surface charge density of the droplet starts to increase. If the coulombic repulsion equals the surface tension of the liquid, the droplet is at the Rayleigh limit and will undergo coulombic fission,[97] whereby the excess charge is distributed on a larger total surface area. However, in this setup the aerosol enters an ionisation chamber before fission can occur (Figure 2). The chamber contains a ^{210}Po-bipolar charger, which ionizes the gas molecules in the air. The excess charge of the droplets is rapidly neutralised via charge exchange and the aerosol attains a well-defined charge distribution as described by the bipolar charging theory of Fuchs.[98] Thus, the excess charge is neutralized before the Rayleigh limit is reached.[23,97] The solvent continues to evaporate and any non-volatile substances present in the spraying solution will form evaporation residues, see Figure 2.

The size of the initial droplets, d_d, is inversely proportional to the conductivity of the sample solution and proportional to the liquid flow rate, Q_L. Thus, the droplet size will decrease with decreasing flow rate and increasing conductivity. The initial droplet diameter can be directly related to the size of the residual particles, d_m, because no columbic fission occurs. The size of droplets is given by:[99]

$$d_d = \frac{1}{c^{1/3}} d_m \tag{8}$$

where c is the concentration of the non-volatile species.

In Figure 3 (left panel) the size distributions of the evaporation residues of a sucrose solution are shown. It can be seen that for higher sucrose concentrations larger evaporation residues were formed. Consequently, it is possible to detect dissolved species by varying the sample concentration as this will cause a shift of the distribution. For solutions of equal conductivity, sprayed at the same Q_L, the initial droplets will be of similar or equal size. This is shown in Figure 3 (right panel) where the initial droplet diameters for the sprayed sucrose solutions, calculated according to Eq. 8, are shown.

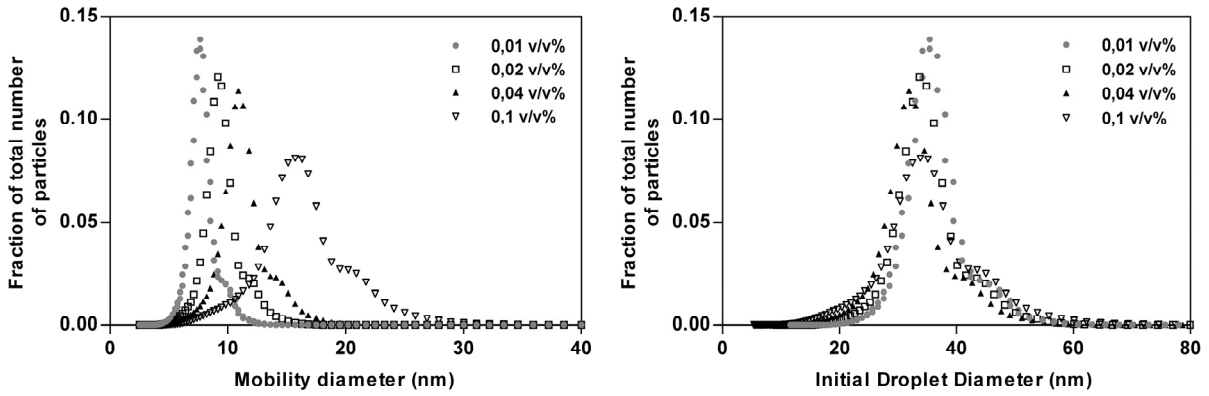

Figure 3. Left panel: The size distributions of sucrose evaporation residues formed from solutions with varying concentration. Right panel: The size distribution of the initial droplets, calculated as described in Eq. 8.

For colloidal analysis, especially when particle aggregation is monitored, it is important to transfer the system from the liquid phase to the gas phase intact. This means that the particles and/or the aggregates should not be ruptured during the transfer process, nor should the transfer create additional aggregation. The second requirement is accomplished by preparing samples, which are sufficiently diluted with respect to the particles, so that the probability that a droplet will contain two or more particles is negligible. Most droplets will contain no particles and they will form small evaporation residues as depicted in the lower part of Figure 2. The evaporation residues can also cause a slight size increase of the colloidal particles. If volatile or semi-volatile electrolyte species, such as HCl or ammonium acetate buffer solution, are used the evaporation residues can be kept at a minimum.

It has been shown that even proteins with weakly associated subunits can be transferred intact in the ES process.[94,95] Hence, the probability that particles are ruptured in the capillary, or during the actual spraying, is low. However, the sample-capillary interaction may cause the particles to adhere to the capillary, and this interaction can distort the observed particle distribution. In some cases, the particles polish the capillary surface, thereby increasing the flow through the capillary. These interactions are dynamic and sample-dependent, which makes exact analysis of the particle concentration in the dispersions rather difficult. Furthermore, the dilution may cause particle dissolution, or shift the equilibrium of other reversible processes, so that the PSDs are altered. Such effects are strongly dependent on the material of the particles. The ES-SMPS size distribution analysis has been shown to work well for a number of colloidal systems,[25,100] including silica,[26] and has successfully been used to monitor the initial aggregation of gold particles.[101]

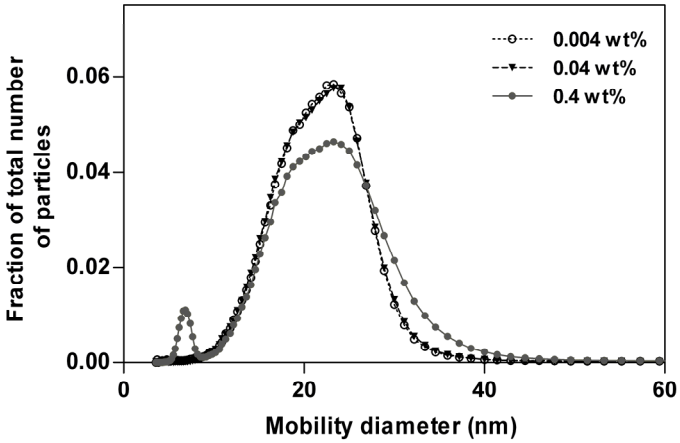

Figure 4. The size distribution of a colloidal silica dispersion at varying sample concentrations.

As can be seen in Figure 4, the highest concentration that can be analyzed without causing aggregation due to the spraying can be determined by varying the sample concentration. For the 0.4 wt% sample, the aggregation that occurs during spraying causes a broadening of the distribution. Moreover, a small evaporation peak appeared for this sample, owing to the fact that the concentration of dissolved silica species in the sample is high enough to form evaporation residues in the detectable size range. For the lower concentrations, *i.e.* those that permit particle transfer without aggregation, the size of the aerosol particles is independent of the sample concentration, because it is determined by the size of the particles that were in the liquid. Thus, the sample concentration dependence can also be used to determine if particulate matter is present in the sample; as the diameter of an evaporation residue will always vary with the concentration, whereas the size of an aerosol particle, which originates from a substrate that was particulate in the liquid phase, is constant for all particle concentrations that do not cause aggregation during the transfer process.

3.1.2 Differential Mobility Analyser

The DMA consists of a grounded metal cylinder with a high voltage rod situated in the centre of the cylinder. When a negative charge is applied to the high voltage rod, an electric field between the rod and the cylinder is created. The polydisperse aerosol is introduced at the top of the DMA adjacent to the outer cylinder. A particle free laminar sheath air flow, Q_S, separates the aerosol flow, Q_A, and the high voltage rod. When the voltage is increased, the electric field accelerates the oppositely charged particles towards the rod in the centre of the DMA. For a given voltage, particles within a specific mobility range will exit the DMA through a slit at the bottom of the rod (Q_A monodisperse). The width of the mobility range depends on the ratio of the aerosol and sheath air flow rates. Particles with mobilities outside the target range will be removed by impaction on the rod or via the excess outflow at the bottom of the DMA (Q_S Excess). A schematic of the long DMA is shown in Figure 5. A nano-DMA was used in Papers I and IV, the working principles are the same but the geometry of the nDMA is optimized for size analysis of small particles, for further information and schematic see Ref 102.

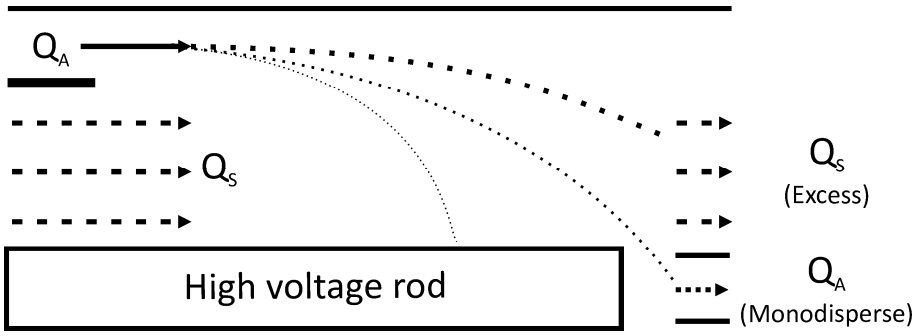

Figure 5. A schematic of the Differential Mobility Analyser (DMA).

The particle electric mobility, Z_p, is a measure of the ease with which a particle with the charge q can be moved by an electric field of field strength E.[5] The mobility can be related to particle size according to:[25]

$$Z_p = \frac{v_e}{E} = \frac{qC_c(d_m)}{3\pi\eta d_m} \tag{9}$$

where v_e is the terminal electrostatic velocity, η is the viscosity of the fluid, and d_m is the mobility diameter of the particle. Small particles are not hindered by the gas molecules to the same extent as larger particles. This causes the small particles to appear even smaller. To correct the mobility of particles below 100 nm the Cunningham slip correction factor, $C_c(d_m)$, is introduced. The mobility diameter of a spherical particle is equal to the physical diameter of the particle, d_p. For non-spherical particles the particle electric mobility, and thereby d_m, can be related to the volume equivalent diameter, d_{ve}, of the particle; *i.e.* the diameter of a sphere with a volume equal to the volume of the non-spherical particle. This gives:[103]

$$Z_p = \frac{qC_c(d_m)}{3\pi\eta d_m} = \frac{qC_c(d_{ve})}{3\pi\eta d_{ve}\chi_t} \tag{10}$$

where d_{ve} is the volume equivalent diameter and χ_t is the orientation averaged dynamic shape factor of the non-spherical particle in the transition regime. Thus, the following relationship between the measured d_m and the volume equivalent diameter of the non-spherical particle is obtained: [103]

$$d_m = d_{ve}\chi_t \frac{C_c(d_m)}{C_c(d_{ve})} \tag{11}$$

Orientation averaged dynamic shape factors can be used for particle Reynolds numbers well below 0.1, because the particle orientation is random.[25] The dynamic shape factors for particles of different shapes and aspect ratios have been reported.[5] In the present investigation, the non-spherical particles were modelled as prolate ellipsoids with a volume given by:

$$V = \frac{4\pi ab^2}{3} \tag{12}$$

where a and b corresponds to the polar and equatorial radii, respectively; the aspect ratio is given by a/b.

3.1.3 Condensation Particle Counter

The size classified particles are counted using a CPC; an optical technique where the light scattered by a particle passing a beam of light is registered. This technique requires aerosol particles in the micrometer size range. Detection of sub-micrometer particles is enabled by mixing the aerosol with a saturated 1-butanol vapor. Subsequently, the mixture enters a cold condenser, where a supersaturated environment is created and the butanol condensates on the particles, thereby causing a rapid size increase. A schematic of the CPC is shown in Figure 6 (left panel).

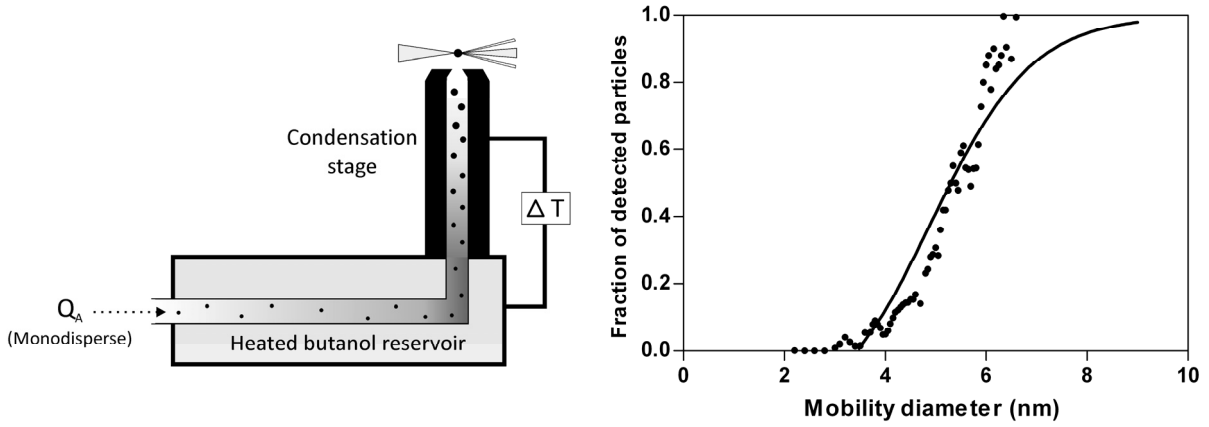

Figure 6. Left panel: A schematic of the Condensation Particle Counter (CPC), where ΔT represents the temperature difference between the butanol reservoir and the condensation stage. Right panel: The detection efficiency curve for the CPC (TSI, model 3010) at ΔT = 25 °C. The results were obtained using an ultra CPC (TSI, model 3025) as reference detector and sprayed insulin particles as size standard. The expression for detection efficiency obtained by Mertes et al. was fitted to the data sets,[104] the fits are shown as solid lines (Figure courtesy of Dr. Magnus Hagström).

The lower detection limit of the CPC (D_{50}) can be tuned by varying the temperature difference (ΔT) between the alcohol reservoir and the condensation stage. A higher ΔT increases the supersaturation and enables detection of smaller particles.[104] For the work presented in this thesis reliable detection of particles below 10 nm is important. Therefore, the maximum temperature difference (25°C), which for this setup corresponds to a D_{50} approximately equal to 5 nm, was used in all experiments. The detection efficiency for the CPC operated at 25°C is shown in Figure 6 (right panel).

Overall, the analysis of aerosol particles in the lower size range (<50 nm) is strongly affected by particle diffusion in the gas phase,[102] which may shift the observed PSDs towards larger sizes.

3.2 Small-Angle X-ray Scattering

In a Small-Angle X-ray Scattering (SAXS) experiment the scattered intensity *I(q)* is measured as a function of the magnitude of the scattering vector *q*; which is given by $q = (4\pi/\lambda)\sin(\theta/2)$ where λ is the wavelength of the X-rays and θ is the scattering angle.[105,106] The X-rays are scattered by the electrons in the sample. Thus, the electron density difference, $\Delta\rho$, in the dispersion, *i.e.* deviations in the local electron density from the average electron density (that of the solvent) in the irradiated volume, is probed. The scattering power of atoms is proportional to their atomic number, and samples with high

electron density, such as silica, will display a high contrast for X-rays. The scattered intensity can be further increased by using an X-ray source with a high flux of radiation, *e.g.* synchrotron radiation. In a synchrotron, the light emitted by electrons orbiting in a magnetic field is used to irradiate the sample.

For a dispersion of monodisperse, homogeneous and spherically symmetric particles *I(q)* can be written as:[107]

$$I(q) = \Delta\rho^2 n V^2 P(q) S(q) \tag{13}$$

where n is the number density of particles and V is the volume of the particles. *P(q)* is the particle form factor which is related to the structure of the particles, *e.g.* their size and shape. *S(q)* is the structure factor, which accounts for the interference of scattering from different particles. Hence, it contains information related to the interactions among the particles; in the dilute case $S(q) \sim 1$. For anisotropic or polydisperse systems *I(q)* cannot be written as a product of the form and structure factors; expressions for *P(q)* for a number of different particle geometries can be found in the literature, see for instance Ref 107.

The particle concentrations of the silica dispersions included in these investigations are high. Thus, it is necessary to account for the *S(q)* contribution to the scattering pattern, because the particle scattering interference can no longer be neglected. The hard-sphere structure factor has been shown to successfully describe the particle-particle interactions in silica dispersions.[108,109] Further, this structure factor is applicable to soft particles and clusters of soft particles.[110,111] The polydispersity of spherical particles can be accounted for with a minimum of additional fitting parameters by constraining the particle radii to follow an analytical distribution function, such as the Schulz distribution function.[70] Thus, by fitting the hard-sphere model,[112] modified to allow for polydispersity or non-spherical shapes of the particles, the variation of particle diameter and polydispersity during aggregation was obtained for unperturbed dispersion/electrolyte reaction mixtures.

3.3 Additional Techniques

3.3.1 Electron Microscopy

Two electron beam imaging techniques, Scanning Electron Microscopy (SEM) and Transmission Electron Microscopy (TEM), have been used to acquire images of the particles and aggregates for size and morphology evaluation. Common to the two techniques is that the interaction of the sample with the electron beam is utilised in the interpretation of the structure.

In SEM a beam with a low acceleration voltage, for the silica measurements ~5kV, is scanned over the sample surface. The beam causes secondary electrons (SE) to be emitted from the topmost layer of the sample. An in-lens detector is used to monitor the amount of SE emitted at a given point and an image of the surface can be constructed. The image contrast depends on the surface topography, since the amount of emitted SE is higher for a curved surface or a sharp edge compared to a flat surface. The samples were prepared either by wet deposition of dilute suspensions, or by impaction of the aerosol particles from the ES,[113,114] on silicon wafers. The latter method permits the

aggregates to be visualized as well, since the aggregation that occurs during wet depositions due to solvent evaporation can be avoided, see Figures 3a and 3b in Paper I.

The TEM samples were prepared by wet deposition of dilute suspensions on a perforated carbon film supported by a TEM copper grid. In a TEM experiment a high voltage beam (~200 kV) is shined through the sample and transmitted electrons are recorded. Here the contrast depends on the atomic weight, density, and thickness of the sample, relative to that of the carbon film. Both techniques are well described in the literature, see for instance Ref 115.

3.3.2 Dynamic Light Scattering

Particles in a suspension constantly collide with the solvent molecules; these collisions cause the particles to move randomly and this random motion is known as Brownian motion. Due to this diffusive particle motion, the intensities of the light scattered by the particles will fluctuate over time. In a Dynamic Light Scattering (DLS) experiment this intensity variation is monitored and an intensity correlation function is determined.[116] The intensity measured at time t_0 is strongly correlated to that measured at $t_0+\delta t$ because the configuration of particles in the illuminated volume is nearly identical. Given time, the particles located in the volume at t_0 will have diffused away; a new particle configuration is established and the intensity measured at *e.g.* t_1 will be totally uncorrelated to that measured at t_0, provided that a sufficient amount of time has elapsed. It follows that the intensity correlation function will decay with time. For monodisperse systems at high dilution the decay will be a pure exponential and the decay rate contains the self diffusion coefficient, D_0, of the particles. Using the Stokes-Einstein equation,

$$D_0 = \frac{k_B T}{6\pi\eta r_H} \tag{14}$$

where η is the viscosity of the solvent, the particle hydrodynamic radius, r_H, can be calculated.[114] For Rayleigh scatterers, the average diffusion coefficient is a Z-average. However, the hydrodynamic diameter obtained form Eq. 14 is a harmonic Z-average diameter, $d_{Z\,harmonic}$, given by:[117]

$$\bar{d}_{Z\,harmonic} = \frac{\sum n_i d_i^6}{\sum n_i d_i^5} \tag{15}$$

The particle diameter measured in a DLS measurement depends strongly on *how* the particles diffuse. The diffusion of a particle can be affected by other particles, for instance, via collisions or electrostatic interactions, but also by the indirect hydrodynamic interactions that arise as surrounding particles diffuse.[116] The hydrodynamic diameter incorporates the hydration of the particle, and can therefore be slightly larger than the dry diameter of a given particle. Other particle properties that affect the diffusion, such as polymers grafted to the particle surface or the gel layer of the silica particles, will influence the obtained diameter.[118,119]

Chapter 4

ES-SMPS Analysis of Colloidal Silica Aggregation

Introduction

In this thesis, the aggregation behaviour of colloidal silica particles in concentrated dispersions has been studied using the ES-SMPS method. Aggregation was induced by addition of electrolyte solutions, and the aggregation proceeded until solid silica gels were formed. Primarily, the work focused on the effects of ion specificity and initial particle morphology on aggregate formation and gel morphology.

A central part of all aggregation investigations (Papers I-III) was the characterisation of the starting materials, *i.e.* the pure dispersions. Combinations of methods, ES-SMPS and SEM in Paper I and ES-SMPS, SEM, and SAXS in Papers II and III, were used in the characterisation. It was observed that the surface properties of the silica particles affected the particle sizes obtained with the various methods. Therefore, a more extensive analysis of the PSD of a pure dispersion, similar to the dispersion used in Paper I, was carried out (Paper IV). A summary of the particle characterization results obtained for the dispersions is given in section 4.1. Furthermore, in Paper I it was observed that the pure silica particles started to dissolve once diluted; the dissolution of the silica particles is discussed in section 4.1.1.

In Paper I a procedure for aggregation analysis with the ES-SMPS setup was developed, and the aggregation of spherical particles in the presence of various alkali ions was monitored. The particle and aggregate diameters were verified with SEM imaging. The SEM samples were prepared by impaction of the aerosol particles on silicon wafers to ensure that no additional aggregation due to sample preparation occurred. The aggregation measurement procedures used in the ES-SMPS experiments are described in section 4.2. Reversible aggregation was observed for this system and the aggregate disintegration was monitored; these results are summarized in section 4.2.2. The ion adsorption sequence at these silica surfaces was determined and a clear ion specific effect on the aggregate disintegration rate was observed. These effects will be discussed conjointly with the ion specific effects observed in Paper III, see below.

To ascertain that the aggregates observed in the diluted samples were the actual aggregates that comprised gel networks of the unperturbed gels, the ES-SMPS measurements were compared with a non-invasive method (Papers II and III). *In situ* SAXS measurements were performed on the undiluted dispersion/electrolyte reaction mixtures. The results concerning the size of the aggregates in the diluted gel samples and undiluted gel structures are summarised in section 4.2.3.

The NaCl induced aggregation of silica dispersions with three different initial particle morphologies was investigated in Paper II. In addition to the dispersion investigated in Paper I, two dispersions with more polydisperse PSDs, one containing spherical particles and the other preaggregates of spherical primary particles, were included. It was observed that the initial particle morphology affected the initial aggregate structures formed, and this could be linked to the composition of the silica surface. These results are shown in section 4.3. A suggestion for the gel network structures that could result from the observed initial aggregates is presented, and compared to existing suggestions for silica gel networks, in section 4.3.3. In Paper III the aggregation of these three dispersions in the presence of KCl and K_2CO_3 was monitored and compared to the results from Paper II. The change in aerosol mass during the aggregation, and after the point of gelation (PoG), was used as an indicator for the rate of gel strength increases in the obtained gels. The ion specific effects observed in Papers I-III, such as aggregate stability and the rate of the gel strength development, are discussed in section 4.4.

4.1 Initial Particle Morphology

The spraying process itself can cause aggregation if the particle concentration in the sample liquid is too high (section 3.1.1). Therefore, all samples, pure dispersions as well as dispersion/electrolyte mixtures, were extensively diluted with ammonium acetate buffer solution prior to analysis. The final sample concentrations were in the range of 0.0025–0.05 wt% SiO_2 depending on the initial particle concentration in the pure dispersions. The size distributions of the pure dispersions investigated in Papers I-III, as obtained using ES-SMPS, are shown in Figure 7.

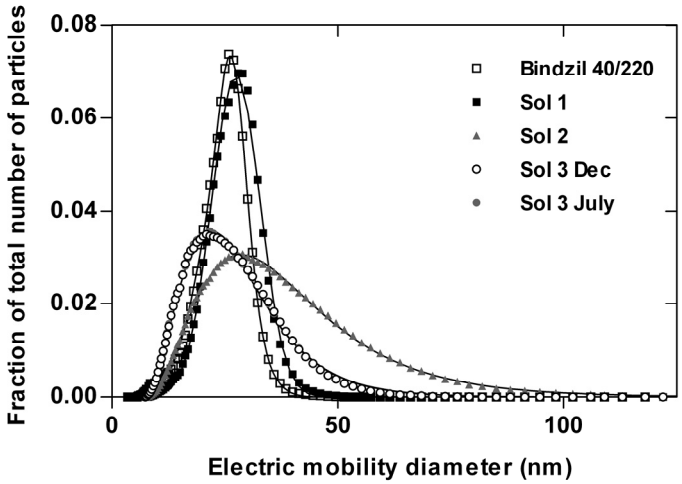

Figure 7. Size distributions of the pure dispersions studied in Papers I-III, fitted distributions are shown as solid lines ($R^2 > 0.99$).

The Bindzil 40/220 batch used in Paper I was newly produced and it showed a tail towards smaller particles. A sum of two Gaussians was fitted to the PSD of this dispersion. A new batch of Bindzil 40/220 was used in Papers II and III, both in the papers and in this thesis the second batch is referred to as Sol 1. This batch had been stored for ~3 months prior to the experiments. The ageing of a dispersion shifts the particle distribution towards larger particles due to Oswald ripening, *i.e.* the smaller particles dissolve more easily and the material is redistributed on the larger particles.[120]

As a result the tail towards smaller particles disappeared and a single Gaussian was sufficient to describe the PSD of Sol 1 satisfactorily (R^2>0.99). The more polydisperse dispersions showed distributions with a tail towards larger particles and log Gaussian distributions were fitted to these PSDs; all fits are shown as solid lines (Figure 7).

In all three papers the size and shape of the silica particles were verified using SEM imaging. Both wet deposition and vacuum particle impaction were used in the sample preparation. It was shown that both batches of Bindzil 40/220 consisted of spherical particles with a narrow size distribution. To differentiate this dispersion from the other more polydisperse systems it will be referred to as monodisperse in this thesis. Furthermore, it was shown that Sol 2 consisted of polydisperse spherical particles and Sol 3 of preaggregated particles; in the thesis the initial particles of Sol 3 will be referred to as preaggregates. The preaggregates were comprised of nearly monodisperse spherical primary particles; overall the preaggregates displayed a polydisperse PSD. A schematic illustration of the particles is given in Figure 8. The shapes of the preaggregated particles (c) ranged from nearly spherical clusters to elongated chains. In the data analysis, they were modelled as prolate ellipsoids, the volume of which is given by Eq. 12.

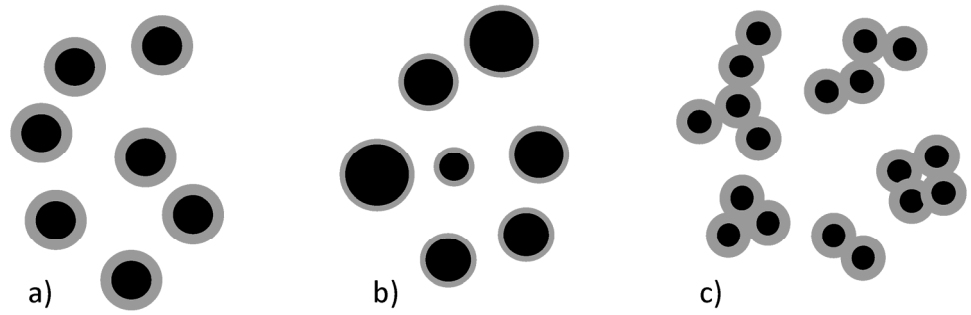

Figure 8. A schematic picture of (a) Sol 1/Bindzil 40/220, (b) Sol 2, and (c) Sol 3. The gel layer is depicted as the light gray circles surrounding the particles.

In Paper II, the pure undiluted dispersions were evaluated using SAXS. For the spherical particle systems the hard sphere model, modified to allow for particle polydispersity, was fitted to the scattering curves; for the preaggregated sample the ellipsoidal hard sphere model was used. From these fits two parameters, the particle diameter D1 and the hard sphere diameter HS, were obtained for the spherical model; whereas three parameters, the particle diameters (D1 and D2) and the hard sphere diameter, were obtained for the ellipsoidal model. The D1 and D2 values corresponds to the physical diameters of the scattering entity, whereas the HS diameters represent the closest distance of approach between two particles in the dispersion. The latter diameter incorporates all features that affect the particle interactions, such as the electrostatic interaction, steric repulsion due to the gel layer, and any possible hydration of the surfaces.

The mean diameters obtained for the pure dispersions with the various methods are summarized in Table 1. All diameters obtained from SEM are arithmetic mean diameters, while the values listed in Paper II for log Gaussian dispersions are the peak diameters of the distributions. To facilitate a correct comparison, the values listed in Table 1 for the dispersions that displayed log Gaussian distributions are arithmetic

mean diameters calculated according to Eq. 5. It can be seen that the d_m-values measured for the dispersions containing spherical particles corresponded well to the physical diameters of the particles, d_p. This is expected since the mobility diameter of a spherical particle can be related to d_p according to Eq. 9. Unfortunately, due to a slight overpressure in the DMA, the mobility diameters originally reported in Papers II and III were ~10% larger compared to the actual physical diameters. The corrected values are shown in parenthesis in Table 1.

Table 1. The particle mean diameters obtained for the pure dispersions.

	ES-SMPS	SAXS		SEM[b]
Sample	**d_m [nm]**	**D1/D2 [nm]**	**HS [nm]**	**d_p [nm]**
Bindzil 40/220	25.4	n/m[a]	n/m	25.7
Sol 1	27.4 (24.7)[c]	15.8	24.8	26
Sol 2	32.0 (28.8)	22.4	26.6	30
Sol 3 Dec	23.6 (21.3)	5.8/22.4	14.0	16/34
Sol 3 July	23.6 (21.2)	6.4/22.4	14.6	n/m

a) Not measured.
b) SEM images were re-evaluated using the software Scanning Probe Image Processor.
c) Values in parenthesis are compensated for the overpressure in the DMA.

The mobility diameter of the non-spherical particles is related to the volume equivalent diameter (d_{ve}) of the particle (section 3.1.2). The d_{ve} of Sol 3 Dec, as calculated from the a and b values measured by SEM imaging, is equal to 21 nm. It can be seen that the mobility diameter of the particles, corrected for the pressure difference, was close to the volume equivalent diameter. Therefore, it was concluded that for these systems it was not necessary to perform the corrections indicated by Eq. 11.

The obtained hard sphere diameters, which correspond to effective interaction diameters, were also comparable with the obtained d_p-values. The D1/D2 diameters, however, did not correspond to any other diameters obtained. This difference was explained by the presence of a gel layer on the silica particle surfaces. A gel layer would most likely have a lower density compared to the core particles. Hence, the scattering contrast of the layer is lower, and the gel layers were, therefore, not detected as part of the scattering particle. However, it was concluded that the gel layer contributed significantly to the particle interaction, because the HS diameters were so close to the physical diameters of the particles. This means that the diameters obtained from SAXS (D1/D2 and HS) corresponded to the core and full particle diameters, respectively, and it was suggested that the extension of the gel layer could be estimated as the difference between the two diameters. In Figure 8 the gel layers are depicted schematically as light grey circles. The gel layer thickness observed for the three dispersions will be discussed further in section 4.1.2, and compared to the results obtained in paper IV for the fourth dispersion.

4.1.1 Particle Dissolution

The total silica concentrations in the dilute samples were below the solubility of silica in water.[121] To ascertain that particle dissolution would not affect the aggregation measurements the dissolution of the pure particles was monitored. The size distribution of a pure Bindzil 40/220 sample (0.0025 wt% SiO_2) was monitored for approximately 2 months; the diluted samples were stored at room temperature in between analysis. In Figure 9 the size distributions immediately after dilution and two months storage are shown (left panel). As the particles dissolve, the concentration of non-volatile silicate species in the solution increases. When the concentration of dissolved silica species has increased sufficiently, evaporation residues in a detectable size range were formed in the spraying process. These can be seen clearly as a small peak around 6 nm in the PSD of the stored sample.

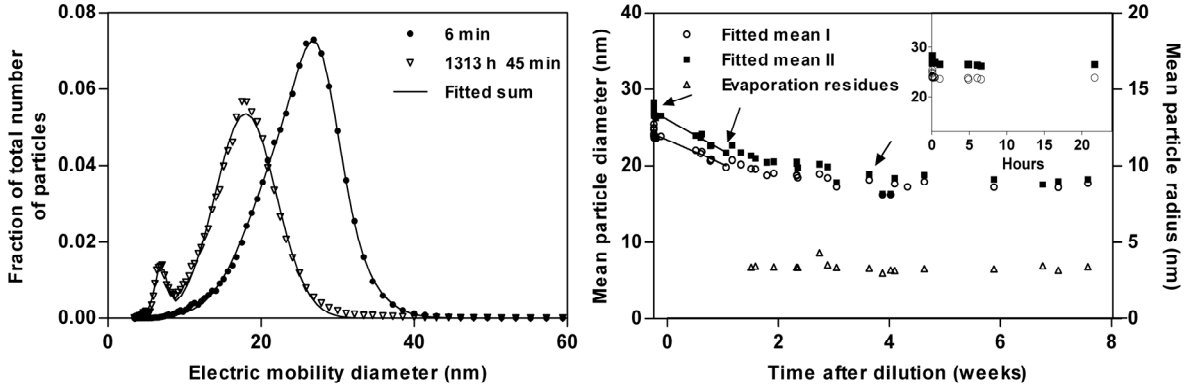

Figure 9. Left panel: The change in the size distribution of pure Bindzil 40/220 during dissolution. Right panel: The corresponding decrease in particle mean diameter during dissolution. The inset shows the decrease during the first 24 hours; the arrows indicate the diameters used to measure the gel layer thickness.

As previously mentioned, a sum of two Gaussian distributions was fitted to the initial distributions of Bindzil 40/220, and when evaporation residues appeared an additional Gaussian was used to account for the third peak. The size of a residue depends on the concentration of non-volatile species in the solution (section 3.1.1). The fact that the size of the residues, once they appeared, remained constant throughout the experiment indicates that a constant concentration of dissolved silica species was attained approximately 2 weeks after dilution. The decrease of the mean particle diameters in the dilute samples is shown in Figure 9 (right panel). The inset shows the change of the mean diameter during the first 24 hours, and it can be seen that the particle diameter remained almost unaffected by the dilution during this time. Hence, it was concluded that the effect of particle dissolution could be neglected provided that the samples were run within a day after dilution.

Initially, when the concentration of dissolved silica species was low, the particles dissolved rapidly. As the dissolution proceeded, the dissolution rate decreased and the mean diameter values reached a plateau. The observed dissolution profile is consistent with results reported in the literature.[122,123] As shown in Figure 9, the mean particle diameter showed a linear initial decrease with time after dilution. A straight line was fitted to the data points corresponding to the initial decrease (solid black line), and the initial dissolution rate was calculated according to Eq. 5 in Paper I. The obtained rate constant was on the order of 10^{-10} mol $m^{-2}s^{-1}$, which is somewhat low compared to those

reported in the literature.[80,123] This is understandable since the experiments presented here were performed at a lower pH (pH 8) and ammonia is known to stabilize the silica surface, thereby reducing the dissolution rate.[7] The observed change in the dissolution rate was attributed to the dissolution of two distinctly different silica phases. Initially, the less polymerised gel layers surrounding the particles dissolved at a relatively high rate. When the gel layers were consumed, the denser particle cores started to dissolve at a slower rate.

4.1.2 Estimated Gel Layer Thickness

The clear distinction of two dissolution regions observed in Paper I indicated that a gel layer was situated at the particle surfaces; this was further supported by the results obtained in Paper II from the SAXS measurements. The existence of a gel layer on the surfaces of silica particles has been suggested by a number of authors.[79,80,122,123] Nevertheless, only a few attempts have been made to estimate the thickness of these layers for various types of silica; for instance, Vigil et al. observed a ~1 nm thick gel layer present at the surface of amorphous silica films.[14] Assuming that the gel layer thickness corresponds to the region displaying fast dissolution, the results from the Bindzil 40/220 dissolution profile (Paper I) suggests that the gel layer was approximately 2 nm thick. However, if the thickness is estimated as the difference between the initial particle diameter and the attained plateau diameter, the gel layer thickness obtained in Paper I was 4.4 nm. These three diameter reference points are indicted by arrows in Figure 9.

In Paper II the gel layer thickness was estimated as the difference between the HS diameters and the D1/D2 values. For Sols 1 and 2 the obtained gel layer thickness was 4.5 and 2.1 nm, respectively. Assuming that the HS diameter obtained for Sol 3 corresponded to an average distance of closest approach for the ellipsoids, and that the side-to-side approach comprised a large part of that average, the HS-values would be a close approximation of the gel layer extension of the primary particles in the preaggregates. This gives a gel layer thickness of 4.1 nm for these particles. The ageing of Sol 3 resulted in larger HS diameters due to Oswald ripening, but the D1-values increased as well, indicating that the inner parts of the gel layer were further polymerized, thereby increasing the size of the core particle. Hence, the thickness of the gel layers was almost equal for the two batches of Sol 3. Furthermore, it was concluded that the gel layer remained intact during the transfer from the liquid phase to the gas phase, and that the ES-SMPS method enabled measurement of the physical diameter of the silica particles.

The presence of a gel layer on the silica surfaces will strongly affect the aggregation of the particles, as will be shown in the following sections. Moreover, it affects the diameters obtained with different methods depending on the capacity of each method to observe the gel layer. In Paper IV a comparative analysis of the PSD of a forth silica dispersion (Bindzil 40/130) was performed using ES-SMPS and DLS as well as SEM and TEM imaging. This dispersion consisted of spherical particles with a narrow size distribution, and was manufactured in a similar way as Bindzil 40/220. However, the dispersion displayed a larger mean diameter and a lower specific surface area, and was with respect to those parameters more comparable to Sol 2.

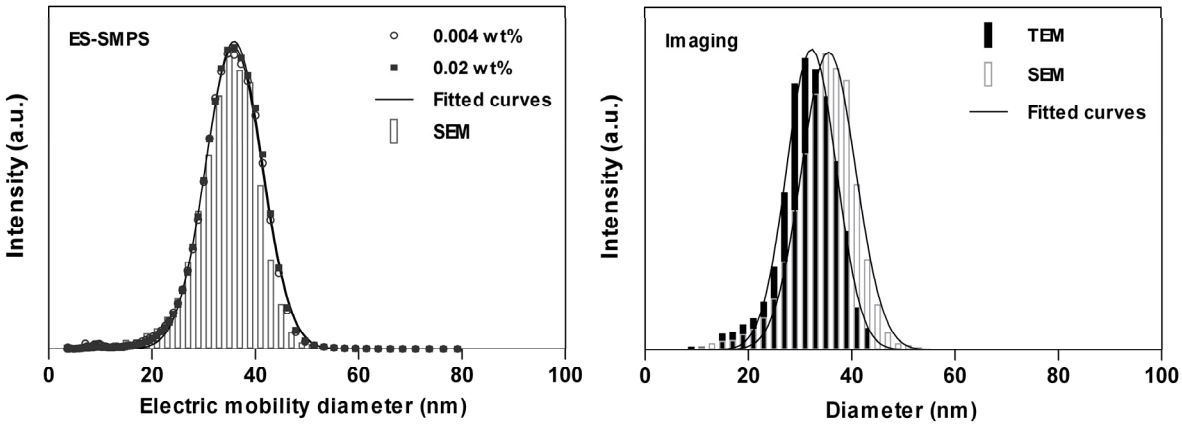

Figure 10. The size distribution of Bindzil 40/130 investigated in Paper IV (sample A), fitted Gaussian distributions are shown as solid lines. The SEM distribution has been added to the ES-SMPS plot to facilitate comparison of the distributions. The TEM and SEM size distributions are based on 1004 and 2624 measured particles, respectively.

The number size distributions, as obtained using SEM, TEM and ES-SMPS, of Bindzil 40/130 are shown in Figure 10. The size distributions showed a main peak centred at ~36 nm in the case of the SEM and ES-SMPS measurements, and for the TEM measurement at 32 nm. A Gaussian distribution could be fitted to the main peak, but the distribution showed a tail toward smaller particles that could not be accounted for by the fit. Therefore, the arithmetic mean diameters of these distributions were calculated according to Eq. 5. From the DLS measurements a harmonic Z-average diameter based on the particle self diffusion was obtained; $d_{Zharmonic}$ values for the number size distributions were calculated according to Eq. 15 to enable comparison with the DLS result. The measured and calculated diameters are listed in Table 2.

Table 2. The calculated mean and $d_{Zharmonic}$ diameters of Bindzil 40/130.

Method	d_{mean} [nm]	$d_{calculated\ Z\text{-}ave}$ [nm]	$d_{measured\ Z\text{-}ave}$ [nm]
ES-SMPS (n=12)	34 ± 0.4	39 ± 0.3	–
SEM (n=1)	35	40	–
TEM (n=1)	32	35	–
DLS (n=14)	–	–	37 ± 0.6

It can be seen that the mean diameter obtained by TEM was approximately 3 nm smaller compared to the mean diameters obtained by ES-SMPS and SEM. The results of the two latter methods agree remarkably well, which is in agreement with the results from Papers I and II. The accuracy of magnification in the SEM and TEM instrumentation was confirmed by measuring a few identical particles in both microscopes (Figure S1 and S2 in the SI of Paper IV). Furthermore, no differences in the size population of the aggregates as compared to the free particles could be detected. Therefore, it is likely that the differences in mean diameter between the two EM methods were due to the sample preparation. However, the exact source of the discrepancy has to be further evaluated in a future study.

The results presented by Tadros and Lyklema indicate that the gel layer is fully penetrable to (at least) the least hydrated ions.[74] Further, Vigil and co-workers suggested that the addition of electrolyte should compress the gel layer owing to the screening of the charges in the layer and on the particle surface.[14] In Paper II it was shown that the extension of the gel layer, as well as the diameter of the core particles, decreased upon electrolyte addition. This result further supports the notion that the gel layers are fully penetrable to ions, even to the more strongly hydrated ions as the decrease of the core diameter was observed for sodium ions. If ions can pass freely through the layer it should be possible for water to flow through the layer at a reduced speed. This should decrease the particle diameter observed using DLS as compared to the full physical diameter measured with ES-SMPS.[118]

In Table 2, it can be seen that the Z-average diameters calculated from the PSDs obtained by ES-SMPS and SEM (the dry diameters) were slightly larger than the hydrated Z-average diameter measured by DLS. A unpaired t-test confirmed that the difference between the calculated and measured Z-average diameters was statistically significant ($p < 0.0001$). In Paper IV it was shown that the gel layer thickness could be approximated from the ratio of the measured and calculated z-averages following the results of Masliyah et al.[118] For the Bindzil 40/130 dispersion a gel layer thickness of ~1 nm was obtained.

Overall, it has been shown that the properties of the gel layer will influence the results obtained in both diffusion related techniques such as DLS, and techniques where the contrast depends on material density such as SAXS.

4.2 Aggregation Measurements

Addition of a sufficient amount of electrolyte to a concentrated silica dispersion results in a destabilization of the system, due to the decrease of the electrostatic repulsion, which leads to particle aggregation. The aggregation proceeds until the system has formed one single aggregate, or a continuous network of aggregates, that spans the entire volume.[81] The resulting solid-like structure is called a gel, and the time after electrolyte addition at which the system solidifies is referred to as the point of gelation (PoG).

In Paper I, a procedure for the ES-SMPS measurements of slow silica aggregation was developed. To obtain comparable conditions in the different dispersion/electrolyte mixtures, the bulk electrolyte concentrations were adjusted to match a specific PoG. In Paper I, the PoG was set to 60 minutes, while in Papers II and III it was set to 40 min and the measurements were continued to approximately 60 min after electrolyte addition in order to monitor the increase of the gel strength. The PoG was determined visually as described in the papers. All experiments were performed at constant temperature (20 °C), and the salt solutions were of sufficiently low concentrations and were added under good agitation so as to not cause local precipitation.

The idea was to maintain a reasonably constant effective surface potential in the presence of various counterions (Li^+, Na^+, K^+, Rb^+, and Cs^+). This should lead to comparable energy barriers, because these are strongly influenced by the electrostatic repulsion, and thereby similar particle contact times in the various mixtures. In Paper I,

the particle electrophoretic mobilities were shown to be comparable or equal in the presence of the various counterions. For a given dispersion, this will yield consistent gel formation kinetics and most likely a consistent gel structure, regardless of the choice of counterion (*cf.* measurements at the CCC). The gel structures formed from dispersions with various initial morphologies are most likely not similar. Nevertheless, the approach enables comparative investigations of systems with diverse initial morphology because all gel networks have evolved within an equivalent time-span. A suggestion for the structure of the gel networks formed will be discussed in section 4.3.3.

4.2.1 Particle Size Distributions in Aggregating Silica Dispersions

The ES-SMPS technique enables differentiation of unaggregated particles and aggregates, because all particles are weighted equally and the unaggregated particles will not be masked by the presence of aggregates. This means that, as the aggregation progresses, bimodal or multimodal size distributions may be observed since the total particle population will be a combination of aggregates and unaggregated particles. The size distribution variation typically observed during silica aggregation is exemplified in Figure 11. Bimodal size distributions were observed during the aggregation sequence for all dispersion/electrolyte mixtures investigated in Papers I-III. The aggregates in the solid gels were also analysed using ES-SMPS; samples of the gels were extracted and diluted prior to analysis, in the text these samples are referred to as gel samples. For example, in Figure 11 the PoG occurred at 43 min and the samples taken at 47, 53, and 57 min are gel samples. Only the aggregates and primary particles detachable from the gel network could be analysed in the these samples.

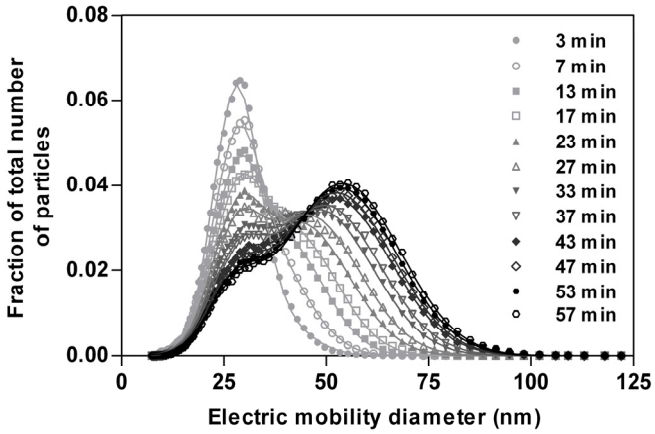

Figure 11. The size distribution variation during NaCl induced aggregation of Sol 1 investigated in Paper II, fits are shown as solid lines.

Occasionally, unimodal size distributions were obtained for the gel samples of the dispersions that formed the more stable gel structures. The gel stability will be further discussed in section 4.4.2. The size distributions were normalized according to the procedure described in Paper I; hence, a fraction of the total number of particles (FTP) was obtained for each size bin and the area under each distribution was equal to 1. To enable analysis of the PSDs acquired during aggregation, sums of two or more theoretical distributions were fitted to the data sets. The theoretical distribution, or distributions in the case of Bindzil 40/220, that best described the PSD of the pure

dispersions (section 4.1), was combined with a Gaussian to account for the aggregate formation, *e.g.* in Figure 11 a sum of two Gaussians was fitted to the size distributions (shown as solid lines in the figure).

4.2.2 Aggregate Disintegration

Preliminary aggregation experiments indicated that the aggregates started to disintegrate rapidly once the samples had been diluted. Therefore, a set of experiments were performed to determine the time-frame in which reliable measurements of the diluted samples could be made. In Paper I, the stability of the silica aggregates was monitored as a function of time after dilution. The decrease in aggregate mean diameter upon dilution is shown in Figure 12.

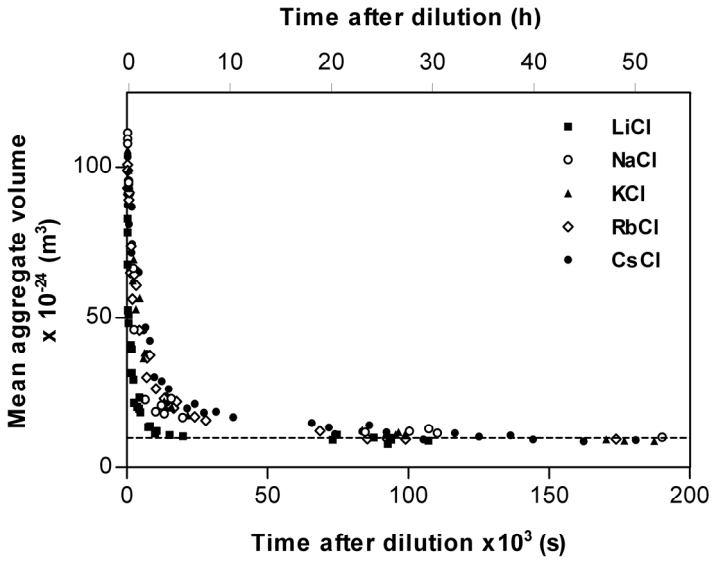

Figure 12. Decrease in mean aggregate volume after dilution for the Bindzil 40/220 aggregates investigated in Paper I. The aggregation was initiated by addition of alkali ions as indicated by the legend. The dashed line equals the volume of an unaggregated particle.

The most important result obtained in these measurements was that the aggregation was, at least initially, completely reversible. Consequently, it was crucial to analyse all samples of the aggregation mixtures immediately after dilution in order to obtain a true representation of the aggregates present in the gelling suspension. The analysis time for each sample was ~10 min. Thus, for a specific dispersion/electrolyte reaction mixture, multiple aggregation experiments were performed. Size distributions were measured at different points during each aggregation run. These results were then compiled to give a complete picture of the overall aggregation process. Furthermore, it was concluded that the aggregate disintegration could be separated from dissolution, since these two processes occurred on vastly different time-scales (*cf.* the initial particle dissolution shown in the inset in Figure 9, right panel).

4.2.3 Aggregate Diameters in the Undiluted Systems

Despite the fact that all ES-SMPS measurements were performed as soon as possible after dilution, a short time delay associated with sample loading could not be avoided. Thus, it could be questioned whether the observed aggregates actually were the aggregate structures that comprised the network of the unperturbed gels, or where the result of an immeasurably rapid disintegration of even larger aggregates. Furthermore, the bimodal size distributions observed for all systems could either be due to the presence of unaggregated particles in the gel structures, or caused by a rapid aggregate disintegration. Therefore, in order to elucidate the composition of the unperturbed mixtures with respect to aggregate sizes, the ES-SMPS measurements were compared with *in situ* SAXS which is a non-destructive method (Papers II and III). Here "non-destructive" refers to the fact that the SAXS measurements were preformed on undiluted mixtures, thus, no aggregate disintegration due to dilution could occur.

The mean aggregate diameters observed in the SAXS and ES-SMPS measurements at the PoG and of the last gel samples are listed in Table 3 (SAXS analysis procedures described in section 4.1). The aggregation was initiated with NaCl. For the dispersions with spherical initial particle morphology, the sizes of the aggregates in the unperturbed gels were close to the aggregate diameters obtained using the ES-SMPS method. Thus, it was shown that the aggregates observed using ES-SMPS were the aggregates that comprised the building blocks of the gel network, as was originally suggested in Paper I. Therefore, it was concluded in Paper II that the results, obtained using the ES-SMPS analysis procedure, were true representations of the aggregates present in the gel structures.

Table 3. The aggregate mean diameters in the gel samples of the NaCl reaction mixtures.

	ES-SMPS	**SAXS**	
Sample	d_m **[nm]**	**D1/D2[a] [nm]**	**HS diameter [nm]**
Sol 1_{PoG}	51.8 (46.6)[b]	50.2	23.8
Sol 1_{final}	54.7 (49.2)	50.4	23.8
Sol 2_{PoG}	66.7 (60.0)	58.4	29.6
Sol 2_{final}	68.0 (61.2)	62.8	30.4
Sol 3 Dec_{PoG}	46.1 (41.5)	5.4/91.2	13.2
Sol 3 Dec_{final}	38.5 (34.7)	5.4/108	17.6
Sol 3 $July_{PoG}$	47.1 (42.4)	5.6/86.8	10.5
Sol 3 $July_{final}$	36.2 (32.6)	5.6/93.5	13.2

a) D1/D2 refers to samples were the ellipsoidal hard sphere model was used. Where only D1 is listed, the hard sphere model was used.
b) Values in parenthesis are compensated for the overpressure in the DMA.

In Paper II, it was also shown that the aggregates observed in the diluted samples throughout the aggregation were approximately equal to the mean aggregates observed in the *in situ* measurements. Only the relative amount of aggregates was higher for the undiluted gels, and it was concluded that the ES-SMPS method monitors the formation of stable aggregates. In the case of Sol 1 it can be seen that the stability of the aggregates increased slightly from the PoG to the final sample, since the mean aggregate

diameter in the diluted samples increased (Table 3). The aggregate and gel stabilities will be further discussed in section 4.4. During the aggregation there was almost no change in the shape or intensity of the curve at higher q (q > 0.4 nm^{-1}) and the small second order peak seen at q = 0.5 nm^{-1} persisted throughout the gelation. This peak was related to the form factor of the primary particles, which suggests that some of the primary particles remain intact all through the aggregation process, which is in line with the previous observations of Zackrisson et al.[124]

Concerning the Sol 3 batches, the calculated d_{ve}-values of the ellipsoidal aggregates at the PoG were equal to 25 and 21 for Sol 3 Dec and Sol 3 July, respectively. These values were calculated using the HS diameters as the equatorial diameter of the ellipsoids, because it was shown in Paper II that these diameters gave a better representation of the preaggregates in comparison to the SEM images. The d_{ve}-values calculated from the SAXS diameters are far from the obtained mobility diameters. For these elongated aggregates the shape factor could influence the measurements, however, even if the shape factor is included according to Eq. 11 the calculated diameters (36 and 32 nm) are smaller than the measured d_m-values. Therefore, it was concluded that, although the SAXS measurements gave a reasonably good estimates of the polar diameters, the equatorial diameters of the aggregates were underestimated. The shape of the aggregates formed in Sol 3 will be discussed further in section 4.3.2.

4.3 Aggregate Formation

The mobility diameter (d_m) measured in the ES-SMPS experiments equals the physical diameter of the particles provided that the particles are spherical. For all other particle shapes, the measured d_m can be related to the volume equivalent diameter, d_{ve}, (section 3.1.2). In Papers II-III this feature was exploited to determine the shape of the initial aggregates: a clear sequential increase of the fraction of total number of particles (FTP) in the size intervals 0-30, 30-40, 40-50, and 50-300 nm was observed for Sol 1. The change of the FTP in these four intervals, observed during the aggregation presented in Figure 11, is shown in Figure 13.

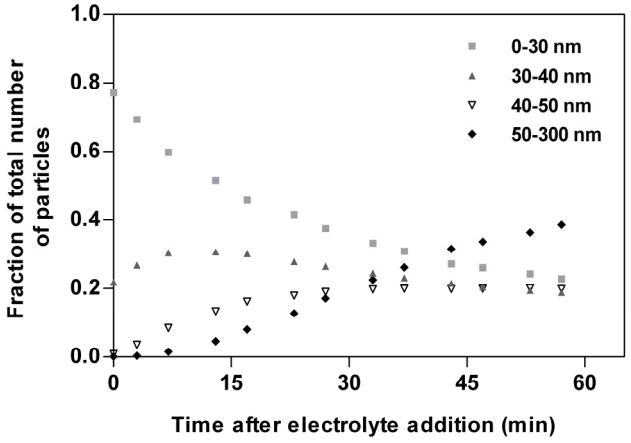

Figure 13. The change in fraction of the total number of particles during the NaCl initiated aggregation of Sol 1 investigated in Paper II.

The d_{ve} of the most probable initial aggregate structures was calculated and compared to the initial changes of the FTP in the four large size intervals. This way, the sequential aggregate formation could be followed and compared for the different initial particle morphologies, this will be explained further in sections 4.3.1 and 4.3.2. The four size intervals identified for Sol 1 were also used in the analysis of Sols 2 and 3, to compare the aggregation processes in the polydisperse systems with that of the monodisperse system. The measured mobility diameters were directly compared to the calculated d_{ve}-values, without including the corrections for particle slip and the dynamic shape factor (section 3.1.2), because the results obtained for the preaggregated particles indicated that in these measurements the d_{ve} was approximately equal to the mobility diameter (section 4.1). In this analysis the mobility diameters have not been corrected for the pressure difference in the DMA, since relative differences were used and the conclusions drawn therefore remain unchanged.

4.3.1 Monodisperse Spherical Particles

The first aggregation step for these particles is the formation of a dimer consisting of two primary particles with a diameter equal or close to the peak diameter of the PSD of the pure dispersion. This step is followed by the addition of a single mean diameter particle to form a trimer. The addition of the third particle can occur at the side of the dimer, at the end of the chain, and at any points in between the two extremes. When a sufficient amount of dimers and trimers have been formed, these will start to aggregate with each other as well as with other unaggregated particles. In Paper I, the shapes of the aggregates were determined using SEM imaging; the SEM samples were prepared by impaction of the sprayed aggregates on silicon wafers, which ensures that no additional aggregation occurred during the sample preparation. It was shown that the largest aggregates consisted of compact nearly spherical clusters of primary particles.

The aggregate shapes observed in Paper I were used as models for the d_{ve} calculations in Paper II. The aggregate structures, composed of 27 nm monomers, resulting from the described sequential build-up, and the corresponding volume equivalent diameters, are depicted schematically in Figure 14.

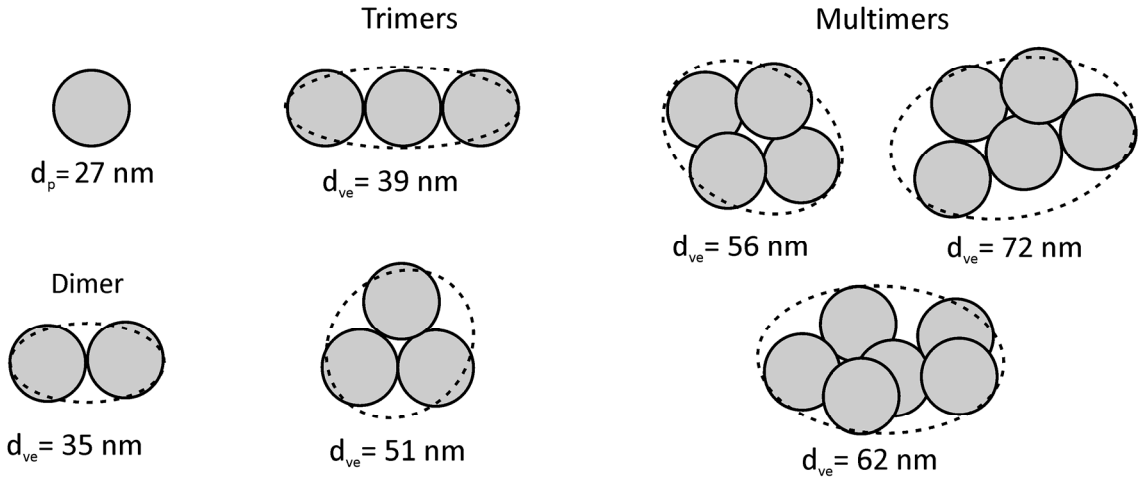

Figure 14. Possible initial aggregate structures in the monodisperse system with the corresponding calculated volume equivalent diameters.

The calculated d_{ve}-values were compared to the changes in the FTP during the aggregation of the monodisperse dispersion (Figure 13). It was found that the increase in the 30-40 nm size range, observed in the early stages for the NaCl induced aggregation of Sol 1, could be explained by the formation of dimers. The increase in the 40-50 nm range was consistent with the formation of trimers, because the size of the trimers most likely ranged in between the two extremes shown in Figure 14. Thus, it was concluded that the dimer formation was followed by the formation of trimers. Moreover, it was shown that the addition of the third particle was equally probable in all directions, as the mean aggregate diameter obtained by SAXS corresponded to a two and a half particle long ellipsoid (Paper II).

Depending on the packing of the particles in the aggregates the size of the aggregates containing more than three particles can vary greatly. However, the volume equivalent diameter of an agglomerate consisting of two of the large aggregates (the multimers) in Figure 14 was ~90 nm, while a linear agglomerate of three large aggregates was ~100 nm. Therefore, it was concluded that the aerosol particles observed in the 50-300 nm size range were aggregates of similar structure as those depicted in Figure 14, because the largest contribution to the FTP in the 50-300 nm range was given by aggregates smaller than 80 nm (Figure 11). The spherical shape of the aggregates was further supported by the fact that a spherical form factor could be fitted to the scattering patterns obtained from SAXS (Paper II).

4.3.2 Polydisperse Spherical and non-Spherical Particles

The change in FTP for Sols 2 and 3 in the presence of NaCl is shown in Figure 15. In the case of Sol 2, the FTP in the size range 0-30 nm started to decrease immediately after electrolyte addition, whereas the FTP in the 30-40 nm range remained constant for a short while before the decrease set in. Initially, a small increase in the 40-50 nm range was observed; as the aggregation progressed aggregate structures contributing to this size interval were formed and consumed at similar rates, wherefore the FTP in the 40-50 nm range remained constant. Furthermore, a rapid increase in the 50-300 nm range was observed immediately after electrolyte addition. During the aggregation the FTP in this size range continued to increase linearly, after the PoG a constant value was attained.

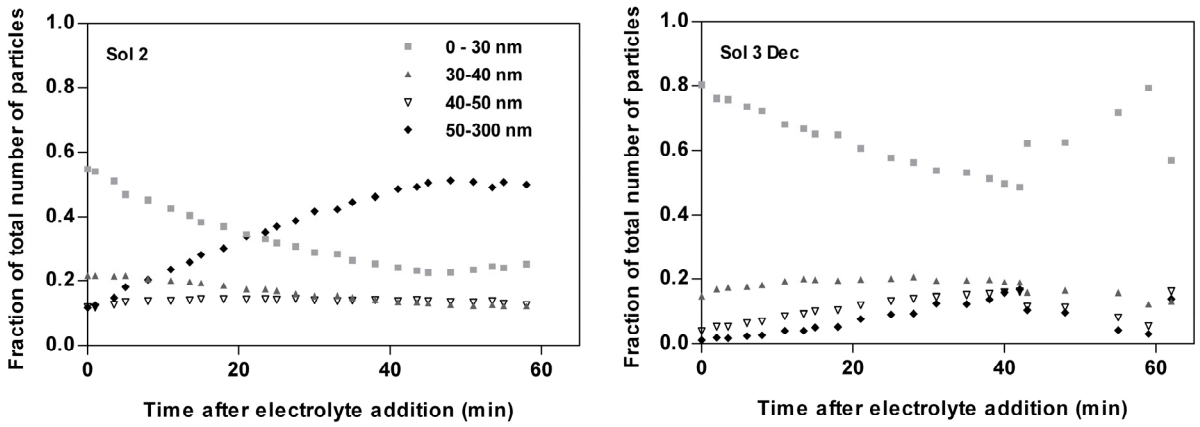

Figure 15. The change in fraction of total number of particles during the NaCl initiated aggregation of Sols 2 and 3 Dec investigated in Paper II. The legend applies to both panels.

A set of possible initial dimers with different sizes arise for Sol 2 owing to the fact that the initial particle population was polydisperse. A schematic of the possible dimer combinations, along with the calculated d_{ve}-values, are shown in Figure 16. The immediate increase in the 50-300 nm range is noteworthy as it can be seen in Figure 16 that a dimer of this size solely can be formed by combining two of the largest particles. In combination with the rapid decrease of particles in the smallest size range, this led to the conclusion that the aggregates initially formed in this dispersion rapidly reached the sizes of trimers or larger. Furthermore, at no point during the aggregation of Sol 2 could a ellipsoidal form factor be fitted to the scattering patterns (*cf.* Sol 1, for which an ellipsoidal form factor could be fitted to the intermediate scattering patterns, see Table 5 in Paper II), which indicated that spherical aggregates were formed from the start.

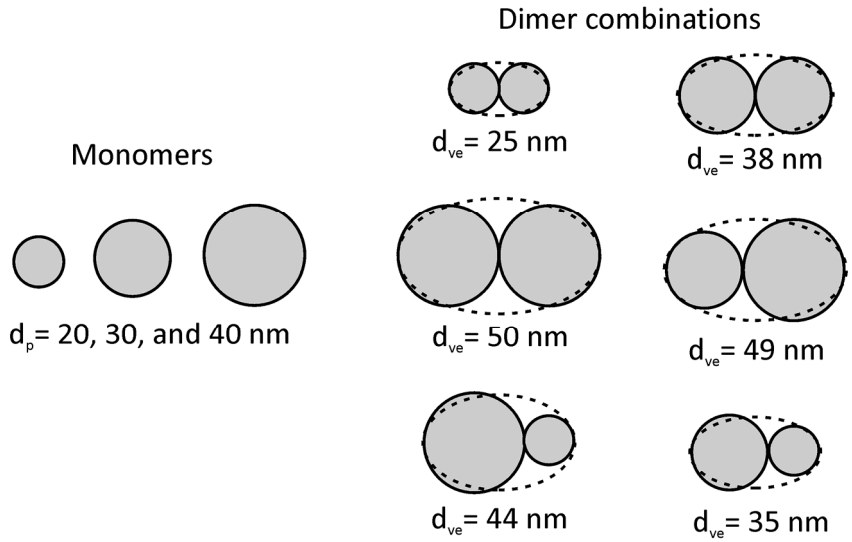

Figure 16. Possible dimer combinations for the polydisperse spherical system (Sol 2) with the corresponding calculated volume equivalent diameters.

The change in the FTP in the four size intervals during NaCl induced aggregation of Sol 3 Dec is shown in Figure 15; a comparable result was obtained for Sol 3 July (Figure 5d in Paper II). As in the case of the other dispersions, the FTP in the size range 0-30 nm started to decrease right after electrolyte addition. Also, it can be seen that the FTP in the larger size intervals increased slowly, while the FTP in the 30-40 nm interval remained almost constant throughout the aggregation. This implies that the aggregates in this size range were formed and consumed at comparable rates. After the PoG an increase of the FTP in the small size range, coupled with decreases in the other size ranges, was observed. This is connected to the increase of the gel stability and will be further discussed in section 4.4.2.

In the case of the preaggregated dispersions (Sol 3 Dec and Sol 3 July), it is not easy to make reasonable assumptions concerning the initial aggregate structures. The preaggregates displayed a range of shapes from straight chains to more compact clusters and any of these shapes can be combined to form the initial aggregates. The mean preaggregate diameter was calculated from SEM images; the preaggregates were modelled as ellipsoid spheroids and equatorial and polar diameters of 16 and 34 nm, respectively, were obtained. This corresponds to a d_{ve} of 21 nm. It could also be concluded

that the average preaggregate consisted of ~4 spherical primary particles with diameters ranging from 10 to 15 nm. Furthermore, an ellipsoidal form factor could be fitted to the scattering patterns obtained throughout the aggregation sequences of these dispersions, indicating that the preaggregates preferentially formed elongated aggregates. Based on these observations, a tentative suggestion for the aggregate structures initially formed in these dispersions is schematically depicted in Figure 17.

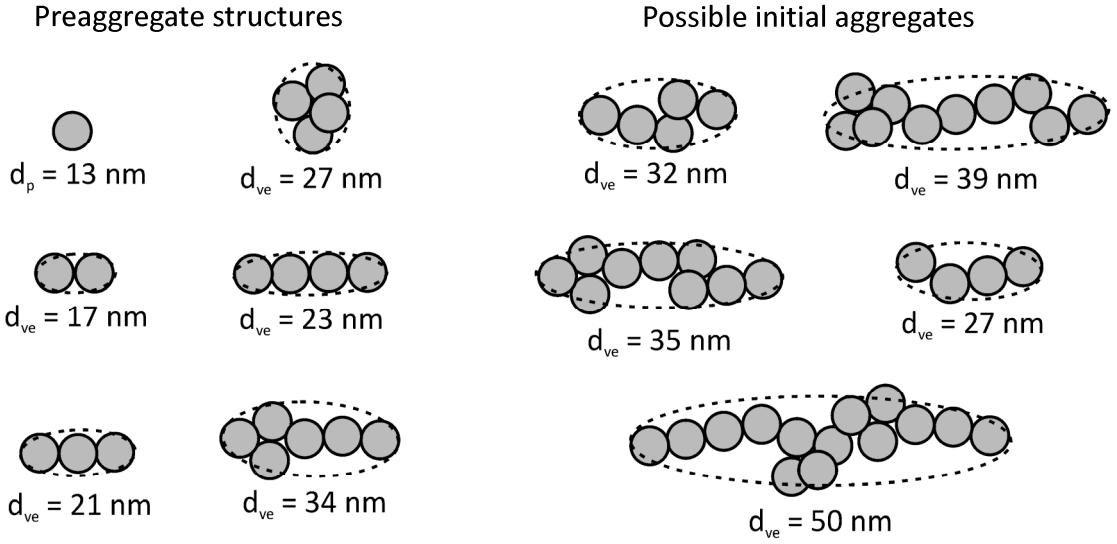

Figure 17. Possible initial aggregate combinations for the preaggregated system with the corresponding calculated volume equivalent diameters.

As is shown in Figure 17, aggregate structures consisting of 2-3 preaggregates can have quite low d_{ve}-values, owing to their elongated shape. More spherical aggregates, containing an equal amount of primary particles, will appear much larger due to their low mobilities. It can be seen that a number of preaggregate combinations, as well as combinations where small preaggregates adhere to newly formed aggregates, results in an aggregate in the 30-40 nm size range. This explains why the FTP in this size interval remained constant throughout the aggregation.

4.3.3 Aggregate Structures and the Resulting Gel Networks

The alternative formation of spherical or elongated aggregates was explained by differences in the surface properties of the particles. In Paper II it was shown that the decrease of the extension of the gel layer after electrolyte addition was most pronounced in the preaggregated dispersions (Sol 3). It was concluded that the gel layers of these dispersions were less cross-linked and therefore more flexible. This indicates that these layers contained a larger number of free silanol groups. Furthermore, the large contraction of the gel layers decreases the steric repulsion, which facilitates a faster aggregation. Sol 1 displayed a less flexible gel layer, and both Sols 1 and 2 had distinctly lower surface areas as compared to Sol 3. Thus, the gel layers of these particles were more polymerised, and therefore, contained fewer free silanol groups.

As was first explained by Usher, particles with an overall repulsive interaction should preferentially build elongated aggregates owing to the fact that the total repulsion is lower for the end-to-end addition of a particle to a chain;[125] but to maintain such a

structure, the aggregates have to be stabilized by rigid interparticle bonds.[20,126] The silica aggregates are thought to be stabilized by the formation of siloxane bonds (section 2.4.2). However, the silica surface is dynamic and siloxane bonds at the surface may be broken and reformed.[15,87] This allows for particle rearrangements in the aggregates to attain energetically more favourable structures (at least while the system is mobile). Recently, it has been shown that long-range electrostatic repulsion combined with a short-range attraction results in the formation of small equilibrium clusters.[20,21]

For the preaggregated dispersion, the elongated aggregate structures could be maintained because a sufficient number of interparticle bonds could be formed rapidly upon particle contact. The elongated structure of the aggregates suggests that less compact gel networks were formed,[126] which could lead to more cross-linked gels. On the contrary, the low number of free silanol groups in Sols 1 and 2 resulted in a slower formation of stable aggregates, because bonds within the gel layer of one particle had to be broken and reformed with the gel layers of the other particles in order to stabilize the aggregate. Consequently, these aggregates could rearrange to attain their equilibrium structures, which were observed in the measurements as spherical aggregates of a specific size. Further, the formation of large spherical aggregates, that were observed early in the aggregation process of Sol 2, is consistent with an aggregation proceeding with the addition of single particles to a growing floc.[126]

The observed aggregate structures contradict the gelation mechanism as proposed by Iler, where the particles are linked together in branched chains to form the gel network. [7] Rather, the network can be envisioned to arise from the agglomeration of the aggregates presented in Paper II. Hence, it consists of two distinctly different structures, the more compact aggregates and the loosely associated agglomerates, and is therefore not a self-similar structure at the whole length scale. The proposed structure is in agreement with the results obtained from simulations,[20] as well as experimental studies on model colloidal systems,[6,21] and dilute silica dispersions.[127] As suggested by Iler, compact aggregates should settle because they are more concentrated with respect to particles as compared to the original dispersion.[7] However, Zackrisson et al.[128] showed that gels, produced from silica dispersions similar to those investigated here, were homogeneous and no sedimentation of the aggregates was observed. This can be explained by the reversible aggregation process suggested here; the aggregates break and reform several times prior to the PoG and only once a sufficient amount of stable aggregates has formed will the gelation occur.

4.4 Ion Specific Effects

Strongly adsorbed ions screen the surface charge more effectively.[50] Therefore, a lower bulk electrolyte concentration is needed to screen the surface to a certain extent. In Papers I-III this was exploited to determine the adsorption sequence of the ions at the silica-water interface. The lower the amount of electrolyte required to attain the predetermined gelation time, the more strongly adsorbed ions. The bulk electrolyte concentrations in the reaction mixtures are listed in the Papers. The direct Hofmeister sequence was observed in all experiments, *i.e.* Cs^+ ions adsorbed more strongly as

compared to Li^+ ions. This is in line with previous results obtained for the silica system.[17,72, 129-131] As a result, the aggregation rate, relative to the amount of electrolyte added, was higher in the presence of structure-breaker ions such as Cs^+ or K^+, see Papers I and III. The observed sequence was explained by the combined effects of the compatibility of the surface and ion water structures, structure-breaker ions preferentially adsorb on structure-breaker surfaces, and the higher ion-surface dispersion interaction for the more polarizable ions (section 2.1.1). In Paper III the hydration of the cations and anions included in the investigation were evaluated using MC simulations. The strong hydration of the Na^+ and CO_3^{2-} ions previously observed was confirmed.[61]

4.4.1 Influence on Aggregate Stability

In paper I the stability of the aggregates in the highly diluted samples was monitored and it was found that the aggregation was initially fully reversible for all counterions investigated. Moreover, the rate of the aggregate disintegration in the highly diluted samples showed a strong counterion dependence. The rate of aggregate disintegration as a function of ion polarisability is shown in Figure 18. It was found that the more strongly adsorbed ions, such as Cs^+ and Rb^+, formed the most stable aggregates. It was concluded that the IIC interaction stabilized the aggregates formed in the presence of the structure-breaker ions since these ions can be fully immersed in the water structure of the silica particles. The ions can adsorb more closely to the surface, whereby the osmotic pressure between the particles is decreased, and the attractive electrostatic pressure contribution becomes dominant (section 2.2.1). Ions that adsorb further from the surface will increase the osmotic pressure between the particles, and the double layer interaction will be repulsive at all interparticle distances. In Paper I this effect was observed for the Li^+ and Na^+ ions as a deviation from the linear increase of the disintegration rate constant with decreasing ion polarisability (Figure 18).

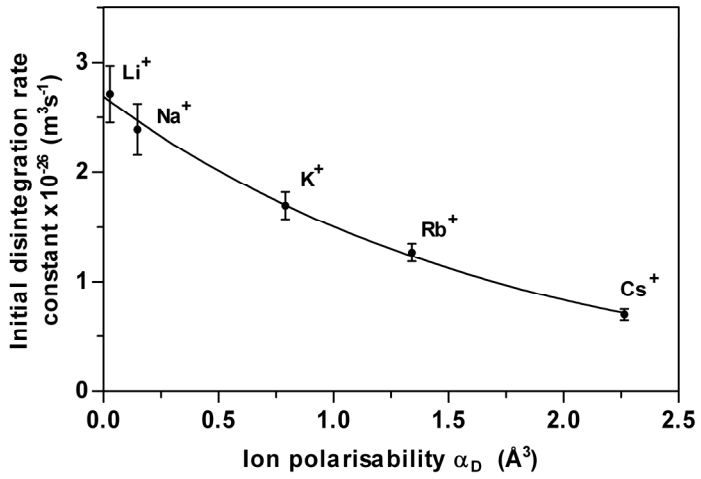

Figure 18. Initial disintegration rate constants as a function of ion polarisability in water. Error bars represent the 95% confidence interval for the rate constants.

Effect of bulk electrolyte concentration. In Paper I the aggregation of the monodisperse dispersion at a longer gelation time was investigated; the PoG was set to 60 minutes whereas it was set to 40 minutes in Papers II and III. The change of FTP in the four size intervals for the KCl, NaCl, and CsCl induced aggregations of Bindzil 40/220 is shown in

Figure 19. These calculations were not part of Paper I, but has been added here to facilitate a comparison of the aggregate stability at different gel times. It can be seen that the slower aggregation followed an aggregate build-up similar to that observed for the aggregation with a 40 minute gelation time, with a sequential increase in the four large size intervals (section 4.3.1). This suggests that the aggregate formation for the monodisperse particle system followed the same general trends independently of the chosen PoG.

Overall, when comparing the 60 and 40 minute PoGs for the NaCl mixtures, the formation of larger aggregates appeared to be slower and the increase in the 50-300 size range started halfway through the 60 minute gelation (*cf.* the 40 minute PoG where they appeared after approximately 10 min, see Figure 13). Also, the relative amount of unaggregated particles was higher for the 60 minute gelation. However, it can be seen that for the 60 minute PoG, stable aggregates were observed progressively earlier in the aggregation process when going from structure-maker to structure-breaker ions so that the change in FTP for the Cs^+ ion was similar to that observed for the 40 minute PoG in the presence of NaCl (Figure 13). These results should be compared with those obtained in Papers II and III for NaCl and KCl, where the change in the FTP was shown to be independent of the choice of counter ion for all dispersions.

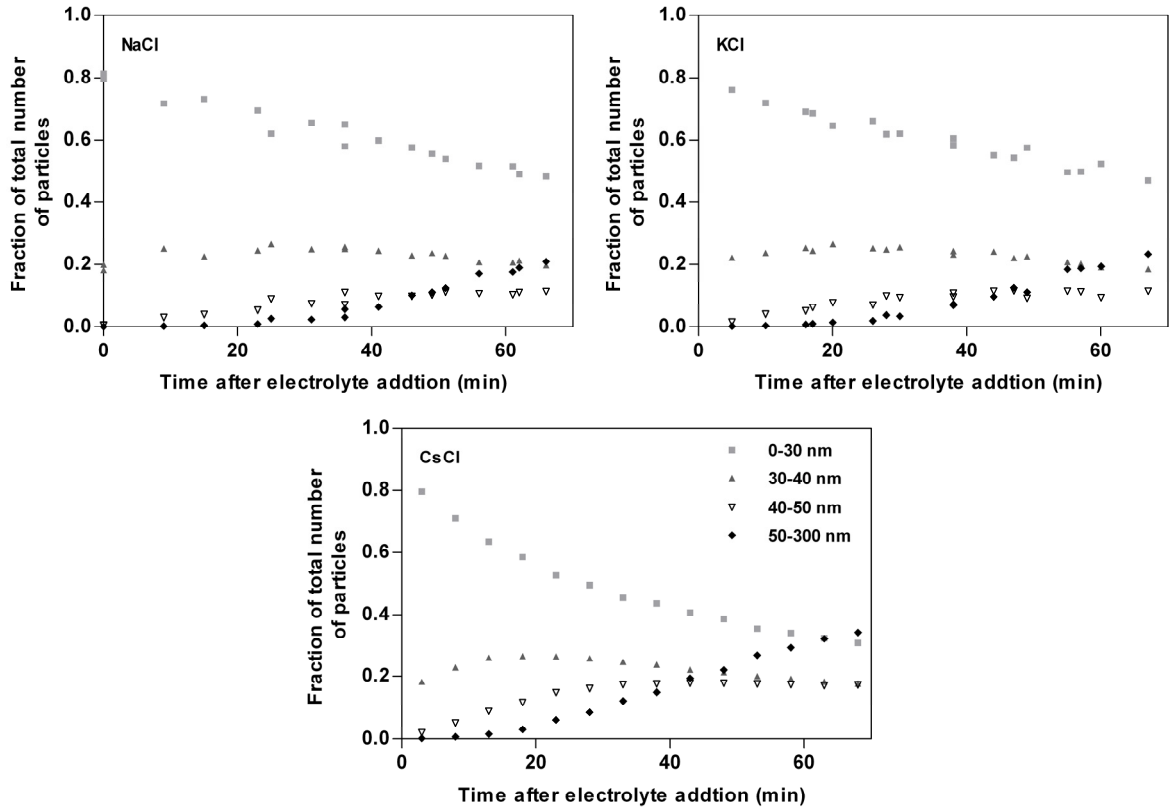

Figure 19. The change of the fraction of total number of particles in the large size intervals for the KCl, NaCl, and CsCl induced aggregations of Bindzil 40/220 investigated in Paper I. The legend applies to all panels.

The ES-SMPS monitored the formation of stable aggregates, and the difference between the NaCl and CsCl FTP results is due to the fact that the unstable aggregates disintegrated before the PSD analysis could be performed. The obtained results indicate that the aggregates formed in the presence of strongly hydrated ions at the lower aggregation rate were less stable as compared to the aggregates formed in the presence of the same ions but at a higher aggregation rate. The observed behaviour can be explained by the fact that the magnitude of the overall IIC interaction is chiefly influenced by the packing of the ions at the interface.[66] When the bulk electrolyte concentration is lower, as in the 60 minute PoG experiments, the contraction of the diffuse layer is less pronounced, resulting in an overall higher ion density at the midplane between two approaching particles. Thus, the interparticle osmotic pressure drives the particles in the aggregates apart. For the 40 minute PoG, where the bulk electrolyte concentrations were higher, the diffuse layers of all the ions were more compressed and the difference between the ions was therefore less obvious. The strong influence of the ion-surface dispersion interaction on the ion adsorption then becomes apparent as the stabilizing effect of the IIC interaction in the CsCl case was comparable to those observed for the NaCl and KCl reaction mixtures with a 40 minute PoG. It should be noted that as the general aggregate formation was the same in the two cases, *i.e.* the aggregation progressed from dimers and trimers to larger more spherical aggregates, only the relative stability of the aggregates appeared to be affected.

4.4.2 Rate of Gel Stability Increase

The results presented so far show that as the aggregation proceeds, more and more stable aggregates are formed. The PoG corresponds to the point where a sufficient amount of stable aggregates connect to form the gel network; after this point, only the particles and aggregates that are detachable from the gel network can be monitored. As the stability of the gel network increases, the amount of detachable particles and aggregates decrease. As long as all particles and aggregates can be transferred, *i.e.* for the samples taken before the PoG, the aerosol mass should be constant because particles in the smaller size intervals are transferred to the larger size intervals. Once the PoG is reached and the amount of detachable particle and aggregates start to decrease, the aerosol mass should decrease as well. In paper III the change in aerosol mass during aggregation was used to measure the rate of gel stability increase.

In Figure 20 the change in aerosol mass during NaCl induced aggregation of Sol 1 is shown, and it can be seen that a drop-off of the aerosol mass was observed after the PoG. However, prior to the PoG an increase of the aerosol mass was observed. This occurs because the aggregates were assumed to be compact particles of the same density as the primary particles in the mass calculations. In reality the aggregates were less dense and the aerosol mass was overestimated which results in the observed mass increase. The increase of the aerosol mass prior to the PoG was used to determine the relative density of the formed aggregates. It was shown that the structure-maker cations and anions formed less dense aggregates.

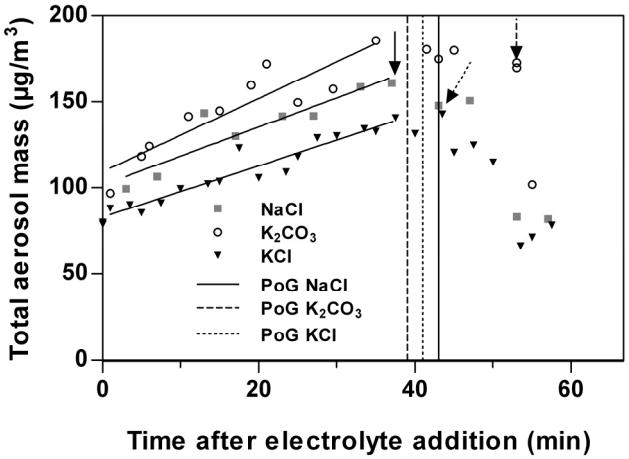

Figure 20. The change in total aerosol mass during aggregation of Sol 1 in the presence of (■) NaCl, (○) K_2CO_3, and (▼) KCl. Vertical lines indicate the points of gelation: NaCl (solid), K_2CO_3 (dashed), and KCl (dotted). The arrows indicate the start of the aerosol mass drop-off.

Moreover, it was found that the general stability of the gels increased in the following order: Sol 1 < Sol 2 < Sol 3 Dec ≈ Sol 3 July, as indicated by the relative drop-off in aerosol mass for each dispersion (Figure 3 in Paper III). The gel stability increase of the Sol 3 samples was so pronounced that only the preaggregates not incorporated in the gel structure could be detected after the PoG for these dispersions. For instance, this can be seen as a decrease of the FTP in the size intervals 30-40, 40-50, and 50-300 nm, coupled with an increase of the FTP in the 0-30 nm size range (Figure 15).

The start of the drop-off in aerosol mass, in relation to the exact PoG, was used as an indication of the rate of the strength increase; an early drop-off corresponds to a faster increase in strength of the gel network. The points where the decrease started are indicated by arrows in Figure 20. The most important result from Paper III was that the rate of the gel stability increase decreased according to the direct adsorption sequence for all the investigated dispersions. This means that the ions that were observed to form the more stable aggregates also displayed a lower rate for the gel stability increase. These results may seem surprising at first, but can be explained by a closer examination of the most important interactions responsible for the aggregate and gel stabilities.

The long-term stability of the gel network, and indeed the aggregates, is provided by the formation of inter-particle covalent bonds according to Reaction 2. However, the development of this stabilising effect is slow owing to the fact that the silica surface is highly dynamic and the siloxane bonds readily break and reform.[15,89] Therefore, the number of inter-particle connections will fluctuate in time. As long as the particles and aggregates can diffuse freely, their interactions may cause the aggregates to break apart if the total number of bonds is momentarily lower. On average, this occurs more often for the aggregates formed in the presence of structure-maker ions, because these aggregates have a lower IIC interaction combined with a higher internal osmotic pressure. The additional stability observed for the aggregates formed in the presence of structure-breaker ions originates from the IIC interaction.

Once the gel network is formed, the particles can no longer diffuse but the inter-particle covalent bonds continue to develop. As can be seen in Reaction 2, this formation is facilitated by an acidic environment. It was concluded that the presence of structure-maker ions enhance the siloxane bond formation since the hydration layers of these ions are more acidic.[132,133]

The results presented in this thesis show that different interactions are important at the various stages of the aggregation and gelation processes. This could potentially explain some of the contradicting results previously obtained for silica, such as the opposing results observed in rheological measurements by Colic et al.[16] and Franks.[17]

Chapter 5

Conclusions

5.1 Concluding Remarks

Electrolyte induced aggregation of concentrated colloidal silica dispersions has been studied using multiple techniques. The initial particle morphology, as well as the electrolytes, were varied, and the effects of these parameters on the aggregate formation and the strength of the gel networks was investigated. Within the project, a procedure for electrospray–scanning mobility particle sizer (ES-SMPS) size distribution measurements during aggregation was developed, and the obtained results were verified using a non-destructive method (SAXS) and electron microscopy. The main conclusions drawn from the investigations can be summarised as follows:

- The ES-SMPS method can be used for the analysis of the aggregation process in concentrated silica dispersions. *In situ* experiments of the unperturbed silica gels confirmed that the aggregates observed using the ES-SMPS method were the aggregates that comprised the building blocks of the gel networks. The relative amount of aggregates were lower in diluted samples as compared to the unperturbed gels, thus the method monitors the formation of stable aggregates.

- A gel layer consisting of protruding and/or adsorbed silicic acid chains was identified on the surfaces of silica particles. The properties of these layers affect the particle diameters obtained with various sizing methods. Methods that rely on particle density and/or the diffusion of the particles will display smaller particle diameters owing to the fact that the gel layer is less dense compared to the core particle and fully permeable to water. It was shown that the silica particles can be transferred to the gas phase with the gel layer intact using the ES technique, and the full physical diameter of the silica particles can therefore be analysed using the ES-SMPS method.

- The aggregation of colloidal silica appears to be a dynamic process where the aggregates may break and reform several times prior to the point of gelation. The gel layers affect the silica aggregation in different ways. Firstly, the steric repulsion caused by the layers increase the stability of the dispersions. Secondly, the degree of polymerisation in the layers influences the interparticle siloxane bond formation, which affects the long-term stability of the aggregates and gel structures. Furthermore, the degree of polymerisation of the gel layer seems to affect the alternative formation of spherical or elongated aggregates, such that silica particles with a more cross-linked gel layer preferentially form spherical aggregates. The gel networks formed from the concentrated silica dispersions

may be envisioned as built-up of agglomerates consisting of smaller, more compact aggregates.

- The direct Hofmeister adsorption sequence was observed for all dispersions included in the investigations and it was shown that the more strongly adsorbed ions form the most stable aggregates. The more strongly hydrated ions, the so-called structure-maker ions, that adsorbed further from the silica surface displayed less stable aggregates due to an increased interparticle osmotic pressure. The particle and aggregate interactions can cause the aggregates to break apart since the number of interparticle covalent bonds fluctuate over time. Once the system is arrested, the effect of the acidic environment surrounding the strongly hydrated ions on the rate of the siloxane bond formation becomes apparent. This was observed as an increased rate of gel strength development in the gels formed in the presence of the strongly hydrated ions. Thus, the results presented in this thesis indicate that, depending on the length- and time-scales probed, different observations with respect to the overall strength of the structures and the ion specificity should be expected. This is an important finding as it may clarify some of the contradicting results previously observed for silica dispersions.

5.2 Future Studies

This thesis shows that the ES-SMPS method is a useful tool in the investigation of the aggregation of concentrated silica dispersions. The method gives valuable information about the initial formation of stable aggregates, as well as important insights to the gel transition and gel stability increase of a system. It should be developed further and implemented in aggregation studies of other colloidal systems. The aggregation of a system previously shown to obey the DLVO-theory would be of special interest as many of the features observed here have been attributed to the non-DLVO behaviour of silica.

The methods to measure the thickness of the gel layer on silica particles developed here should be further tested; for instance, a more thorough investigation of various silica products should be conducted and the results should be compared to the specific surface area of the products.

In addition, it would be interesting to continue the investigation of the effects of the structure-maker ions on the rate of gel stability increase. The measurements of the silica aggregation in the presence of Li^+ and Cs^+ ions should be compared to *in situ* measurements of the gel strength increase and to the absolute strength of the gels.

Acknowledgement

Droppen.

En droppe droppad i livets älv
har ingen kraft att flyta själv
Det ställs ett krav på varenda droppe:
Hjälp till att hålla de andra oppe!

- Tage Danielsson

Well this is it…The End ☺. Five wonderful, challenging, and stimulating years has gone by, and I have been very fortunate to have had a huge support from supervisors, colleagues, friends, and family. I could not have done this without you! Particularly, I would like to thank:

The **Department of Chemistry** – I will be forever thankful that I was accepted as a "free-mover" PhD student and that **Jan Petterson**, **Zareen Abbas**, **Magnus Hagström** and **Staffan Wall** accepted to be my supervisors. You have all had the courage to support my ideas and to let me endeavour on my own, yet your doors have always been open should I need advice. The Swedish tax payers are gratefully acknowledged for financing these fantastic years! Anna Fock at Petnoga did the proof-reading of this thesis.

Jan – One can't be down when Jan is around! Your spirit and fantastic sense of humour has really enlightened my time as a PhD student. Thank you for keeping me on track when I have tried to do *everything* at once.

Zareen – You have helped me to see the colloidal world from a theoretical perspective, for this I am most grateful. I have really enjoyed discussing both science and other worldly matters with you.

Magnus – You introduced me to the lovely field of aerosol science and to the electrospray technique ☺. With a tremendous patience you stood by me while I made all the mistakes one has to make in order to fully learn something new.

Staffan – You showed me the wonderful world of colloidal chemistry and without you I would not stand here today, thank you!

Inger Jansson – You have been my mentor, colleague and dear friend for many years. Over the years we have talked (and laughed) a lot about work as well as other more important things. You have given me perspective and valuable advice in both work and personal life. I am very grateful that you invited me to participate in the SAXS study.

Caterina Camerani – My companion in FISH-he*l ☺. Thank for helping me with the SAXS measurements and analysis, and for teaching me about SAXS in general. I have truly enjoyed working with you.

Eka Chemicals is gratefully acknowledged for financial support and for an endless supply of the central ingredient of this thesis –colloidal silica. To my former colleagues at Industrial Specialties, especially **Catarina**, **Peter**, **Bosse**, **Bozena**, **Jenny L**, **and Lars**, thank you so much for all your help and support, and for opening your labs to me.

Johan Bergenholtz – Thank you very much for all your help with SAXS and DLS related questions and for truly nice science discussions over the years. **Jeanette Ulama** I look forward to our collaboration this coming fall and I hope you will forgive me for moving away.

Stefan Gustafsson – Skilled SEM operator! Thank you very much for all the fruitful discussions, collaborations, and for a lot of help over the years.

Environmental Nanochemistry group and in particular **Martin, Jani, and Julian** – Thank you for a really nice and fruitful collaboration.

Atmospheric Science group – To former and present members, thank you ever so much for seven magnificent years! Your help and support, and our friendly and enjoyable "atmosphere" in the coffee room has meant the world to me. Special thoughts goes to my room-mate **Kent (Kenshi) Salo** for hysterically funny times ☺, my diploma worker **Elin Löfström Engdahl** for your good sprits and hard work, and to **Benny Lönn** for your technical skills and for speaking your mind.

Electrochemistry group – A big thank you to **Elisabet Ahlberg** and her group for inviting me to participate in their group meetings and scientific discussions; a special thanks goes to my zombie-friend **Jenny pH** for a very nice collaboration during the summer (watch out for the pea shooter…☺).

I am indebted to the administrative staff at the Department of Chemistry: **Ingrid**, **Kerstin**, **Hannah**, **Malin**, **Eliza** and **Ann**. I also wish to express my gratitude to **Lennart Sjölin** and **Åke Nilsson** for being such wonderful teachers.

PhD Student Council – I was privileged to participate in this fantastic group of dedicated PhD students, who has done such a good job over the years. Thank you for great discussions and a really nice time.

Ingela, Isabella, Johanna, and Lisa (Stressgänget) – When things are tough it is good to have someone to confide in; thank you for open discussions and really nice, relaxing stress lunches ☺.

Jan-Erik Jönsson and **Kerstin Jonasson** – The best secondary and high school chemistry teachers there are. I could not have had a better start.

AnnKatrin, **Anne-Therese** and **Fia** – Gals gals gals! (Interestingly, also the unit of acceleration in the cgs system, but here refers to girl or woman.) What would I do without you? Thank you for lengthy talks, good nights out, endless coffee sessions, and for always *always* being there for me!

Till min familj: **Mamma**, **Pappa**, **Farmor**, **Mormor**, **Morfar**, **Tova och Amanda**; för ert stöd, för att ni ger mig perspektiv på livet och för att ni tror på mig – ett mycket stort TACK!

Staffan – The love and light of my life! The BIGGEST thank you for your enormous patience, for being understanding and supportive, and for taking care of me while I've been writing. I promise I will never be boring again ;), with humongous love from ACG^3 to PB^2W!!!! >:*<

References

(1) Dickinson, E. (ed.) *Food Colloids – Interactions, Microstructure, and Processing;* The Royal Society of Chemistry; Cambridge, 2005.

(2) Tadros T. F. (ed.) *Colloids and Interface Science Series, Vol. 4 Colloids in Cosmetics and Personal Care*; Wiley-Vch Verlag; Weinheim, 2008.

(3) Tadros T. F. (ed.) *Colloids and Interface Science Series, Vol. 6 Colloids in Paints*; Wiley-Vch Verlag; Weinheim, 2010.

(4) Hunter, R. J. *Foundations of Colloid Science*; Oxford University Press Inc.; New York, 2001.

(5) Hinds, W. C. *Aerosol Technology Properties, Behavior, and Measurement of Airborne Particles*; Wiley Interscience; New York, 1999.

(6) Lu, P. J.; Zaccarelli, E.; Ciulla, F.; Schofield, A. B.; Sciortion, F.; Weitz, D. A. *Nature* **2008**, *453*, 449.

(7) Iler, R. K. *The Chemistry of Silica*; Wiley Interscience; New York, 1979.

(8) Lei, H.; Luo, J. *Wear* **2004**, *257*, 461.

(9) Bergna, H. E. (ed.) *The Colloid Chemistry of Silica*; American Chemical Society; Washington DC, 1994.

(10) Funehag, J.; Gustafson, G. *Tunnelling Underground Space Tech.* **2008**, *23*, 1.

(11) Funehag, J.; Gustafson, G. *Tunnelling Underground Space Tech.* **2008**, *23*, 9.

(12) Gallagher, P. M.; Lin, Y. *J. Geotech. Geoenviron. Eng.* **2009**, *135*, 1702.

(13) Howells, A. R.; Zambrano, P. J.; Collinson, M. M. *Anal. Chem.* **2000**, *72*, 5265.

(14) Vigil, G.; Xu, Z.; Steinberg, S.; Israelachvili, J. *J. Colloid Interface Sci.* **1994**, *165*, 367.

(15) Yaminsky, V. V.; Ninham, B. W.; Pashley, R. M. *Langmuir* **1998**, *14*, 3223.

(16) Colic, M.; Fisher, M. L.; Franks, G. V. *Langmuir* **1998**, *14*, 6107.

(17) Franks, G. V. *J. Colloid Interface Sci.* **2002**, *249*, 44.

(18) Trompette, J. L.; Meireles, M. *J. Colloid Interface Sci.* **2003**, *263*, 522.

(19) Trompette, J. L.; Clifton, M. J. *J. Colloid Interface Sci.* **2004**, *276*, 475.

(20) Sciortino, F.; Buldyrev, S. V.; De Michele, C.; Foffi, G.; Ghofraniha, N.; La Nave, E.; Moreno, A.; Mossa, S.; Saika-Voivod, I.; Tartaglia, P.; Zaccarelli, E. *Comp. Phys. Comm.* **2005**, *169*, 166.

(21) Campbell, A. I.; Anderson, V. J.; van Duijneveldt, J. S.; Bartlett, P. *Phys. Rev. Lett.* **2005**, *94*, 208301.

(22) Bordi, F.; Cametti, C.; Sennato, S. *Chem. Phys. Lett.* **2005**, *409*, 134.

(23) Kaufman, S. L.; Skogen, J. W.; Dorman, F. D.; Zarrin, F.; Lewis K. C. *Anal. Chem.* **1996**, *68*, 1895.

(24) Kaufman, S. L. *J. Aerosol Sci.* **1998**, *29*, 537.

(25) Song, D. K.; Lenggoro, I. W.; Hayashi, Y.; Okuyama, K.; Kim, S. S. *Langmuir* **2005**, *21*, 10375.

(26) Lenggoro, I. W.; Xia, B.; Okuyama, K.; Fernandez de la Mora, J. *Langmuir* **2002**, *18*, 4584.

(27) Hunter, R. J. *Foundations of Colloid Science* pp. 5-6; Oxford University Press Inc.; New York, 2001.

(28) Israelachvili, J. N. *Intermolecular and surface forces*; Elsevier Inc.; Oxford, 2011.

(29) Dobiáš, B.; Qiu, X.; von Rybinski, W. *Solid-Liquid Dispersions*; Marcel Dekker Inc.; New York, 1999.

(30) Derjaguin, B. W.; Landau, L. *Acta Physicochim. U.R.R.S.* **1941**, *14*, 633.

(31) Verwey, E. J.; Overbeek, J. Th. G. *Trans. Faraday Soc.* **1946**, *42*, 117.

(32) Israelachvili, J. N. *Intermolecular and surface forces* p. 316; Elsevier Inc.; Oxford, 2011

(33) Israelachvili, J. N. *Intermolecular and surface forces* p. 312; Elsevier Inc.; Oxford, 2011

(34) Hamaker, H. C. *Physics* **1937**, *4*, 1058.

(35) Hunter, R. J. *Foundations of Colloid Science* p. 543; Oxford University Press Inc.; New York, 2001.

(36) Norrish, K.; Rausell-Colom, J. A. *Clay Clay Minerals* **1961**, *10*, 123.

(37) Donners, W. A. B.; Rijnbout, J. B.; Vrij, A. *J. Colloid Interface Sci.* **1977**, *61*, 249.

(38) Israelachvili, J. N.; Adams, G. E. *J. Chem. Soc. Faraday Trans. 1*, **1978**, *74*, 975.

(39) Pashley, R. M.; McGuiggan, P. M.; Ninham, B. W.; Brady, J.; Evans, D. F. *J. Phys. Chem.* **1986**, *90*, 1637.

(40) Hartley, P. G.; Larson, I.; Scales, P. J. *Langmuir* **1997**, *13*, 2207.

(41) Pashley, R. M.; Kitchener, J. A. *J. Colloid Interface Sci.* **1979**, *71*, 491.

(42) Pashley, R. M. *J. Colloid Interface Sci.* **1981**, *83*, 531.

(43) Israelachvili, J. N.; Pashley, R. M. *Nature* **1983**, *306*, 249.

(44) Hofmeister, F. *Arch. Exp. Pathol. Pharmakol.* **1888**, *24*, 247. (English translation: Kunz, W.; Henle, J.; Ninham, B. W. *Curr. Opin. Colloid Interface Sci.* **2004**, *9*, 19.)

(45) Craig, V. S. J.; Ninham, B. W.; Pashley, R. M. *Nature* **1993**, *364*, 317.

(46) Lo Nostro, P.; Ninham, B. W.; Lo Nostro, A.; Pesavento, G.; Fratoni, L.; Baglioni, P. *Phys. Biol.*, **2005**, *2*, 1.

(47) Weissenborn, P. K.; Pugh, R. J. *J. Colloid Interface Sci.* **1996**, *184*, 550.

(48) Jungwirth, P.; Tobias, D. J. *J. Phys. Chem. B* **2002**, *106*, 6361.

(49) Boström, M.; Williams, D. R. M.; Ninham, B. W. *Biophys. J.* **2003**, *85*, 686.

(50) Lyklema, J. *Adv. Colloid Interfac.* **2003**, *100-102*, 1.

(51) Lyklema, J. *Chem. Phys. Lett.* **2009**, *467*, 217.

(52) Grahame, D. C. *J. Electrochem. Soc.* **1951**, *98*, 343.

(53) Gierst, L.; Herman, P. *Fresen. J. Anal. Chem.* **1966**, *216*, 238.

(54) Ninham, B. W.; Yaminsky, V. *Langmuir* **1997**, *13*, 2097.

(55) Netz, R. R. *Eur. Phys. J. E* **2001**, *5*, 189.

(56) Karraker, K. A.; Radke, C. J. *Adv. Colloid Interfac.* **2002**, *96*, 231.

(57) Tavares, F.W.; Bratko, D.; Blanch, H. W.; Prausnitz, J. M. *J. Phys. Chem.* **2004**, *108*, 9228.

(58) Boström, M.; Deniz, V.; Franks, G. V., Ninham, B. W. *Adv. Colloid Interface Sci.* **2006**, *123-126*, 5.

(59) Dumont, F.; Warlus, J.; Watillon, A *J. Colloid Interface Sci.* **1990**, *138*, 543.

(60) Marcus, Y. *J. Solution Chem.* **1994**, *23*, 831.

(61) Marcus, Y. *Chem. Rev.* **2009**, *109*, 1346.

(62) Gierst, L.; Vandenberghen, L.; Nicolas, E.; Fraboni, A. *J. Electrochem. Soc.* **1966**, *113*, 1025.

(63) Parsons, D. F.; Boström, M.; Maceina, T. J.; Salis, A.; Ninham, B. W. *Langmuir* **2010**, *26*, 3323.

(64) López-León, T.; Santander-Ortega, M. J.; Ortega-Vinuesa, J. L.; Bastos-González, D. *J. Phys. Chem. C* **2008**, *112*, 16060.

(65) Porus, M.; Labbez, C.; Maroni, P.; Borkovec, M. *J. Chem Phys.* **2011**, *135*, 064701.

(66) Kjellander, R. *Ber. Bunsenges. Phys. Chem.* **1996**, *100*, 894.

(67) Greberg, H.; Kjellander, R. *J. Chem. Phys.* **1998**, *108*, 2940.

(68) Labbez, C.; Jonsson, B.; Skarba, M.; Borkovec, M. *Langmuir* **2009**, *25*, 7209.

(69) Hunter, R. J. *Foundations of Colloid Science* p. 214; Oxford University Press Inc.; New York, 2001.

(70) Kotlarchyk, M.; Chen, S-H.; Huang, J. S.; Kim, M. W. *Phys. Rev. A* **1984**, *29*, 2054.

(71) Hunter, R. J. *Foundations of Colloid Science* p. 224; Oxford University Press Inc.; New York, 2001.

(72) Stöber, W.; Fink, A.; Bohn, E. *J. Colloid Interface Sci.* **1968**, *26*, 62.

(73) Foissy, A.; Persello, J. *Surface Group Ionization on Silicas* In The Surface Properties of Silicas p. 368, Legrand, A. P. (ed.); John Wiley & Sons Ltd.; West Sussex, 1998.

(74) Tadros, Th F.; Lyklema, J. *J. Electroanal. Chem.* **1968**, *17*, 267.

(75) Hunter, R. J. *Foundations of Colloid Science* p. 501; Oxford University Press Inc.; New York, 2001.

(76) Brinker, C. J.; Scherer, G. W. *Sol-Gel Science* p. 626; Academic Press Inc.; San Diego, 1990.

(77) Miranda, P. B.; Xu, L.; Shen, Y. R.; Salmeron M. *Phys. Rev. Lett.* **1998**, *81*, 5876.

(78) Manciu, M.; Calvo, O.; Ruckenstein, E. *Adv. Colloid Interface Sci.* **2006**, *127*, 29.

(79) Healy, T. W. *Stability of Aqueous Silica Sols* In *The Colloid Chemistry of Silica* p. 156, Bergna, H. E. (ed.) American Chemical Society; Washington DC, 1994.

(80) Kobayashi, M.; Juillerat, F.; Galletto, P.; Bowen, P.; Borkovec, M. *Langmuir* **2005**, *21*, 5761.

(81) Allen, L. H.; Matijević, E. *J. Colloid Interface Sci.* **1969**, *31*, 287.

(82) Allen, L. H.; Matijević, E. *J. Colloid Interface Sci.* **1970**, *33*, 420.

(83) Trompette, J. L.; Meireles, M. *J. Colloid Interface Sci.* **2003**, *263*, 522.

(84) Walldal, C.; Wall, S.; Biddel, D. *Colloids Surf. A: Physichem. Eng. Aspects* **1998**, *131*, 203.

(85) Lin, M. Y.; Lindsay, H. M.; Weitz, D. A.; Ball, R. C.; Klein, R.; Meakin, P. *Nature* **1989**, *339*, 360.

(86) Dumont, F. *Stability of Sols* In *The Colloid Chemistry of Silica* pp. 143-146, Bergna, H. E. (ed.); American Chemical Society; Washington DC, 1994.

(87) Depasse, J. *J. Colloid Interface Sci.* **1997**, *188*, 229.

(88) Depasse, J.; Watillon, A. *J. Colloid Interface Sci.* **1970**, *33*, 430.

(89) McPherson, J. W. *J. App. Phys.* **2006**, *99*, 083501.

(90) Zeleny, J. *Phys. Rev.* **1917**, *10*, 1.

(91) Cloupeau, M.; Prunet-Foch, B. *J. Aerosol Sci.* **1994**, *25*, 1021.

(92) Fenn, J. B.; Mann, M.; Meng, C. K.; Wong, S. F.; Whitehouse, C. M. *Science* **1989**, *246*, 64.

(93) Cole, R. B. (ed.) *Electrospray Ionization Mass Spectrometry*; Wiley Interscience; New York, 1997.

(94) Veenstra, T. D. *Biophysical Chemistry* **1999**, *79*, 63.

(95) Loo, J. A.; Berhane, B.; Kaddis, C. S.; Wooding, K. M.; Xie, Y.; Kaufman, S. L.; Chernushevich, I. V. *J Am Soc Mass Spectrom* **2005**, *16*, 998.

(96) Cloupeau, M.; Prunet-Foch, B. *J. Electrostatics* **1989**, *22*, 135.

(97) Kaufman, S. L. *Anal. Chim. Acta* **2000**, *406*, 3.

(98) Hussin, A.; Scheibel, H. G.; Becker, K. H.; Porstendörfer, J. *J. Aerosol Sci.* **1983**, *14*, 671.

(99) Chen, D-R.; Pui, D. Y. H.; Kaufman, S. L. *J. Aerosol Sci.* **1995**, *26*, 963.

(100) Abbas, Z.; Perez Holmberg, J.; Hellström, A.-K.; Hagström**,** M.; Bergenholtz, J.; Hassellöv, M.; Ahlberg, E. *Colloids Surf. A: Physichem. Eng. Aspects* **2011**, *384*, 254.

(101) Tsai, D.-H.; Pease III, L. F.; Zangmeister, R. A.; Tarlov, M. J.; Zachariah, M. R. *Langmuir* **2009**, *25*, 40.

(102) Fissan, H.; Hummes, D.; Stratmann, F.; Büscher, P.; Neumann, S.; Pui, D. Y. H.; Chen, D. *Aerosol Sci. Tech.* **1996**, *24*, 1.

(103) DeCarlo, P. F.; Slowik, J. G.; Worsnop, D. R.; Davidovits, P.; Jimenez J. L. *Aerosol Sci. Tech.* **2004**, *38*, 1185.

(104) Mertes, S.; Schröder, F.; Wiedensohler, A. *Aerosol Sci. Tech.* **1995**, *23*, 257.

(105) Feigin, L. A.; Svergun, D. I. *Structure Analysis by Small-Angle X-Ray and Neutron Scattering*; Plenum Press; New York, 1987.

(106) Narayanan, T.; Gomez, M.; Nogales, A.; Garcia-Gutierrez, M. C.; Ezquerra, T. A. *Applications of Synchrotron Light to Scattering* and *Diffraction in Materials and Life Sciences, Lecture Notes in Physics*; Springer; Berlin, 2009, Vol. 776, pp 133-156.

(107) Pedersen, J. S. *Adv. Colloid Interface Sci.* **1997**, *70*, 171.

(108) Qiu, D.; Cosgrove, T.; Howe, A. M.; Dreiss, C. A. *Langmuir* **2006**, *22*, 546.

(109) Gommes, C.; Blacher, S.; Goderis, B.; Pirard, R.; Heinrichs, B.; Alié, C.; Pirard, J.-P. *J. Phys. Chem. B* **2004**, *108*, 8983.

(110) Stieger, M.; Skov Pedersen, J.; Lindner, P.; Richtering, W. *Langmuir* **2004**, *20*, 7283.

(111) Posselt, D.; Skov Pedersen, J.; Mortensen, K. *J. Non-Cryst. Solids* **1992**, *145*, 128.

(112) Ashcroft, N. W.; Lekner, J. *Phys. Rev.* **1966**, *145*, 83.

(113) Liu, P.; Ziemann, P. J.; Kittelson, D. B.; McMurry, P. H. *Aerosol Sci. Tech.* **1995**, *22*, 293.

(114) Svane, M.; Hagström, M.; Pettersson, J. B. C. *Aerosol Sci. Tech.* **2004**, *38*, 655.

(115) Egerton R. F. *Physical Principles of Electron Microscopy—An Introduction to TEM, SEM, and AEM*; Springer Science & Business Media Inc.; New York, 2005.

(116) Finsy, R. *Adv. Colloid Interface Sci.* **1994**, *52*, 143.

(117) Finsy, R.; De Jaeger, N. *Part. Part. Syst. Charact.* **1991**, *8*, 187.

(118) Masliyah, J. H.; Neale, G.; Malysa, K.; van de Ven, T. G. M. *Chem. Eng. Sci.* **1987**, *42*, 245.

(119) Zackrisson, M.; Bergenholtz, J. *Colloids Surf. A: Physichem. Eng. Aspects* **2003**, *225*, 119.

(120) Ratke, L.; Voorhees, P. W. *Growth and Coarsening: Ostwald Ripening in Material Processing*; Springer-Verlag; Berlin, 2002.

(121) Gunnarsson, I.; Arnórsson, S. *Geochim. Cosmochim. Acta* **2000**, *64*, 2295.

(122) Holt, P. F.; King, D. T. *J. Chem. Soc.* **1955**, *3*, 773.

(123) Yates, D. E.; Healy, T. W. *J. Colloid Interface Sci.* **1976**, *55*, 9.

(124) Zackrisson, A. S.; Pedersen, J. S.; Bergenholtz, J. *Colloids Surf. A: Physichem. Eng. Aspects* **2008**, *315*, 23.

(125) Usher, F. L. *Roy. Soc. Proc A* **1929**, *125*, 143.

(126) Sutherland, D. N. *J. Colloid Interface Sci.* **1967**, *25*, 373.

(127) Hermawan, M.; Bushell, G.; Bickert, G.; Amal, R. *Int. J. Miner. Process.* **2004**, *73*, 65.

(128) Zackrisson, A. S.; Martinelli, A.; Matic, A.; Bergenholtz, J. *J. Colloid Interface Sci.* **2006**, *301*, 137.

(129) Sonnefeld, J.; Göbel, A.; Vogelsberger, W *Colloid Polym. Sci.* **1995**, *273*, 926.

(130) Tikhonov, A. M. *J. Phys. Chem. C.* **2007**, *111*, 930.

(131) Dishon, M.; Zohar, O.; Sivan, U. *Langmuir* **2009**, *25*, 2831.

(132) Depasse, J. *J Colloid Interface Sci.* **1999**, *220*, 174.

(133) Bernasconi, L.; Baerends, E. J.; Sprik, M. *J. Phys. Chem. B* **2006,** *110,* 11444.